© 2015. Published by The Company of Biologists Ltd | Development (2015) 142, 2781-2791 doi:10.1242/dev.123539

RESEARCH ARTICLE

Fat1 interacts with Fat4 to regulate neural tube closure, neural progenitor proliferation and apical constriction during mouse brain development

Caroline Badouel[1,*], Mark A. Zander[2,3,*], Nicole Liscio[1], Mazdak Bagherie-Lachidan[1], Richelle Sopko[4], Etienne Coyaud[5], Brian Raught[5], Freda D. Miller[2,3,6] and Helen McNeill[1,6,‡]

ABSTRACT

Mammalian brain development requires coordination between neural precursor proliferation, differentiation and cellular organization to create the intricate neuronal networks of the adult brain. Here, we examined the role of the atypical cadherins Fat1 and Fat4 in this process. We show that mutation of *Fat1* in mouse embryos causes defects in cranial neural tube closure, accompanied by an increase in the proliferation of cortical precursors and altered apical junctions, with perturbations in apical constriction and actin accumulation. Similarly, knockdown of *Fat1* in cortical precursors by *in utero* electroporation leads to overproliferation of radial glial precursors. Fat1 interacts genetically with the related cadherin Fat4 to regulate these processes. Proteomic analysis reveals that Fat1 and Fat4 bind different sets of actin-regulating and junctional proteins. *In vitro* data suggest that Fat1 and Fat4 form cis-heterodimers, providing a mechanism for bringing together their diverse interactors. We propose a model in which Fat1 and Fat4 binding coordinates distinct pathways at apical junctions to regulate neural progenitor proliferation, neural tube closure and apical constriction.

KEY WORDS: Fat cadherins, Mammalian cortex development, Apical constriction, Brain, Neural tube defects, Radial glial precursor

INTRODUCTION

Neural tube closure defects (NTDs) are very common and severe congenital malformations that affect ~1/1000 pregnancies (Mitchell, 2005). The neural tube forms by thickening of the dorsal surface ectoderm, which folds up and joins at the midline. Neural tube closure requires tight coordination of numerous processes, including polarized apical constriction, proliferation and apoptosis (reviewed by Copp, 2005). Neural tube closure in the cranial region is specifically dependent on actin dynamics. It is believed that the actinomyosin cytoskeleton underlying the apical surface of the neuroepithelium is important for either dorsal lateral hinge point formation or the convergence of neurofolds, or both. This is illustrated by the fact that many actin-regulating proteins, such as Mena (Enah – Mouse Genome Informatics) and Vasp, when deleted from the developing mouse embryo lead to a defect in cranial neural tube closure (reviewed by Copp, 2005; Copp and Greene, 2010). Genes regulating neural progenitor proliferation, neuronal differentiation and apoptosis are also essential for proper neural tube closure, particularly in the cranial region. In addition, mutations in planar cell polarity (PCP) genes lead to severe NTDs, in which the neural tube fails to close along the entire length of the neural tube (Tissir and Goffinet, 2013).

After closure of the neural tube, the mammalian cortex is formed from radial neuroepithelial cells, and later radial glial precursors, the predominant cortical precursor cells during corticogenesis. Radial glial precursors are bipolar cells with apical adherens junctions that line the lateral ventricle, forming an epithelial structure. These radial precursors can divide symmetrically or asymmetrically, producing either an intermediate neuronal progenitor, or a neuron that can then migrate along the radial precursor basal process to form the new neuronal layers of the cortex (Fig. 1A).

Fat cadherins are extremely large cell adhesion molecules, with more than 30 cadherin repeats. In *Drosophila* there are two Fat family cadherins: Fat and Fat-like (Kugelei – FlyBase). Fat regulates PCP, and restricts tissue growth through the Hippo pathway (reviewed by Sopko and McNeill, 2009; Staley and Irvine, 2012) and via regulation of metabolism (Sing et al., 2014). It has been proposed that Fat binding to another atypical cadherin, Dachsous, leads to dimerization and processing of Fat, ultimately activating an intracellular cascade (Feng and Irvine, 2009; Sopko et al., 2009). Although less studied, Fat-like has been shown to regulate the organization of actin stress fibers in the ovarian follicle cell (Viktorinova et al., 2009). Four mammalian Fat genes have been identified, designated *Fat1* to *Fat4*. Fat is most similar to Fat4, and Fat-like is most similar to Fat1-3. Whereas Fat2 is expressed only in the adult, Fat1, 3 and 4 and their ligands dachsous 1 and 2 are expressed during embryogenesis and are found throughout the developing central nervous system (Rock et al., 2005).

Fat1 mutants die around birth, probably from failure in glomerular slit formation in the kidneys (Ciani et al., 2003). In addition to kidney defects, *Fat1* mutants have deformed eyes and craniofacial malformations, with low incidence of holoprosencephaly, which has not been well described or characterized. Fat1 is also involved in muscle formation, and linked to facioscapulohumeral dystrophy (Caruso et al., 2013). At the cellular level, Fat1 interacts with Mena/Vasp proteins to regulate cell migration and actin dynamics in cell culture (Moeller et al., 2004; Tanoue and Takeichi, 2004; Hou and Sibinga, 2009). However, the relevance of this interaction to development has not been explored.

By contrast, more is known about Fat4. Embryos mutant for *Fat4* exhibit PCP defects, suggesting that the polarity function of Fat is

[1]Lunenfeld-Tanenbaum Research Institute, Mount Sinai Hospital, Toronto, Ontario, M5G 1X5, Canada. [2]Neuroscience and Mental Health Program, Hospital for Sick Children, University of Toronto, Toronto, Ontario, Canada. [3]Institute of Medical Sciences, University of Toronto, Toronto, Ontario, Canada. [4]Department of Genetics, Harvard Medical School, Boston, MA 02115, USA. [5]Princess Margaret Cancer Centre, University Health Network, Toronto, Ontario, M5G 2M9, Canada. [6]Department of Molecular Genetics, University of Toronto, Toronto, Ontario, M5S 1A8, Canada.
*These authors contributed equally to this work

‡Author for correspondence (mcneill@lunenfeld.ca)

Received 20 February 2015; Accepted 6 July 2015

Development (2015) 142, 2781-2791 doi:10.1242/dev.123539

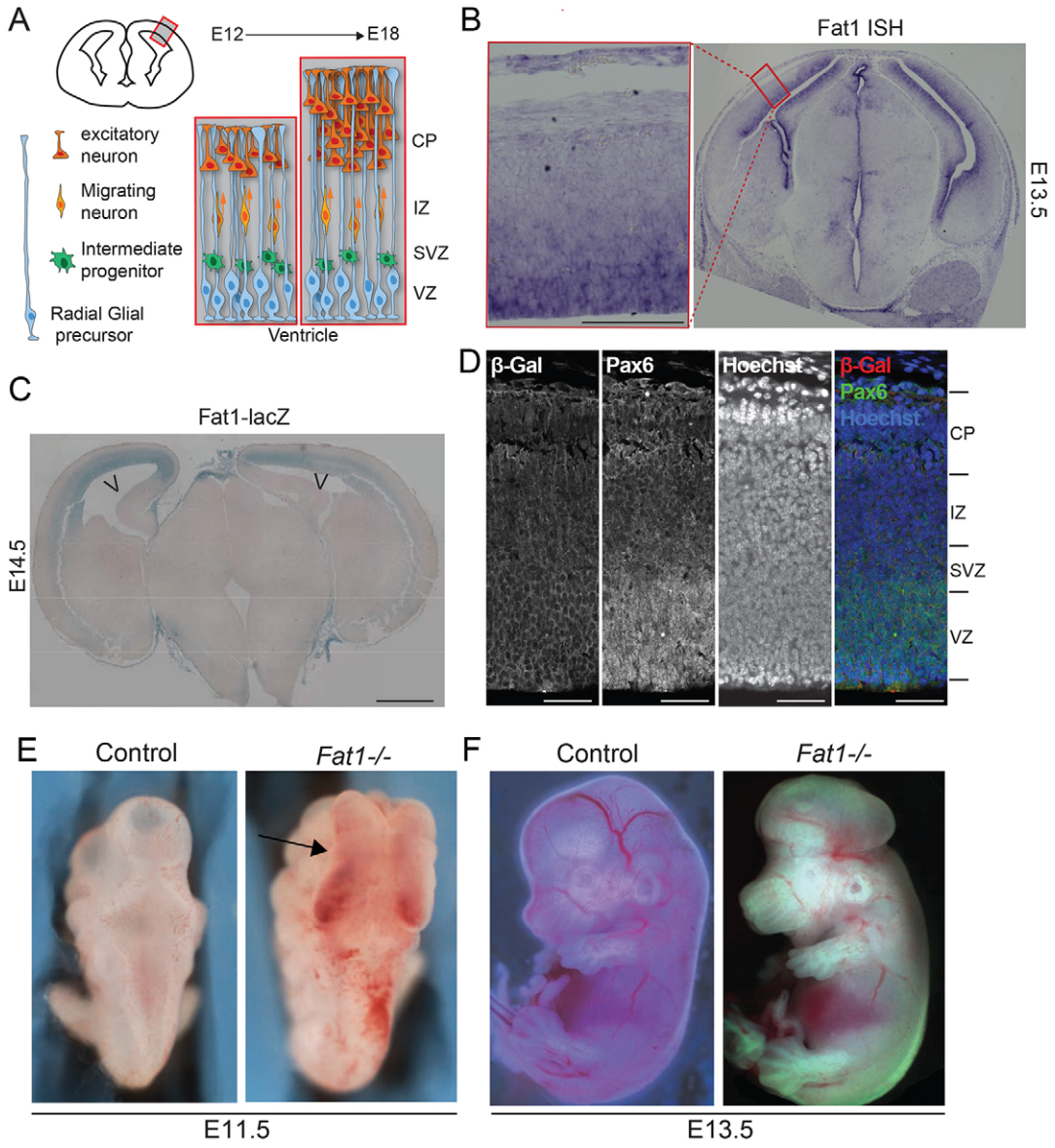

Fig. 1. Loss of Fat1 leads to cranial neural tube defects. (A) Schematic of mouse cortex development. Radial precursors are bipolar cells that can divide symmetrically to self-renew, or asymmetrically, producing either an intermediate neuronal progenitor, or a neuron that can migrate along radial precursor basal processes to form the new neuronal layers of the cortex. (B) *Fat1* expression in a coronal section from E13.5 brain revealed by *in situ* hybridization. The left panel is a magnification of the cortex. Note that *Fat1* is strongly expressed in the VZ of the cortex containing radial precursors. (C) Coronal section through E14.5 $Fat1^{+/-}$ brain stained for β-galactosidase to assess *Fat1-lacZ* expression. (D) Coronal section through E14.5 brain stained for β-galactosidase (red) and the cortical precursor marker Pax6 (green) and with Hoechst (blue). (E) Dorso-anterior view of an E11.5 $Fat1^{-/-}$ embryo and a control sibling. Note that anterior neural folds are open in $Fat1^{-/-}$ (arrow). (F) E13.5 $Fat1^{-/-}$ embryo showing exencephaly and control sibling. VZ, ventricular zone; SVZ, subventricular zone; IZ, intermediate zone; CP, cortical plate; V, ventricle. Scale bars: 100 µm in B; 500 µm in C; 40 µm in D.

conserved (Saburi et al., 2008; Mao et al., 2011). The Fat4 intracellular domain can rescue most of the PCP defects of *fat* mutant flies (Pan et al., 2013). Although structure/function analyses suggest that the *Drosophila* growth regulatory domain is not conserved in Fat4 (Matakatsu and Blair, 2012; Zhao et al., 2013; Bossuyt et al., 2014), Fat4 restricts the growth of neuronal progenitors in the developing chick neural tube (Van Hateren et al., 2011). Moreover, *Fat4* mutations are associated with Van Maldergem syndrome, a recessive multiple malformation syndrome in humans that includes periventricular neuronal heterotopia (Cappello et al., 2013). Fat4 localizes at the subapical domain of neuronal cortical precursors in the mouse, where it regulates the height of the subapical region (Ishiuchi et al., 2009).

Here, we show that loss of *Fat1* leads to exencephaly in mouse embryos and to an increase in radial precursor proliferation in the cortex. Knockdown of Fat1 in the developing cortex *in utero* also leads to overproliferation of radial precursors. At the cellular level, we show that Fat1 is important for actin accumulation at the apical junctions of radial precursors and is needed for apical constriction. We confirm that Fat1 and Fat4 interact genetically in exencephaly, and show additive effects on proliferation in knockdown experiments. Our proteomic analyses reveal that Fat1 and Fat4 bind dramatically different sets of actin-regulating and junctional proteins. As our co-immunoprecipitation experiments suggest that Fat1 and Fat4 form cis-heterodimers, we propose a model in which Fat1 and Fat4 dimer formation

Development (2015) 142, 2781-2791 doi:10.1242/dev.123539

coordinates distinct pathways at apical junctions to regulate brain development.

RESULTS

Loss of Fat1 leads to exencephaly

Fat1 is present in the developing central nervous system with strong expression in the neocortex (Ciani et al., 2003). We analyzed in detail Fat1 expression in the developing cortex throughout neurogenesis from E11.5 to E18.5 (Fig. 1B,C; supplementary material Fig. S1A-C). Interestingly, this analysis revealed that Fat1 expression is strongest in the germinal region known as the ventricular and subventricular zone (VZ and SVZ) of the developing cortex at mid-neurogenesis (E13-14) (Fig. 1B,C; supplementary material Fig. S1B). Towards the end of neurogenesis, at E18.5, Fat1 expression can also be seen in the upper neuronal layer of the cortex (supplementary material Fig. S1C). Taking advantage of *Fat1-lacZ* mice, we performed β-galactosidase staining to show that Fat1 expression colocalizes strongly with the radial precursor markers Pax6 and nestin in the neocortex (Fig. 1D; supplementary material Fig. S1D). This expression pattern suggests that Fat1 is involved in cortical development, possibly regulating cortical precursors.

To elucidate the role of Fat1 in cortical development, we analyzed *Fat1* mutant embryos. Neural tube closure normally concludes at ~E10 with cranial fold and caudal neuropore closure. At E11.5, we find that ~40% (6/17) of *Fat1*$^{-/-}$ embryos in a CD-1 genetic background show open and separated anterior neural folds (Fig. 1E). This defect is specific to the cranial region, since *Fat1*$^{-/-}$ embryos have a closed posterior neural tube. Cranial NTDs lead to exencephaly, characterized by an expansion of the brain outside the skull, which is visible as early as E13-14 (Fig. 1F). At E14.5, ~40% (16/37) of CD-1 *Fat1*$^{-/-}$ embryos are exencephalic.

Increased radial precursor cell proliferation in *Fat1* exencephalic mutants

A role for Fat1 in corticogenesis was investigated further by analyzing *Fat1* mutant brains at later time points. We first characterized the overall morphology of *Fat1* exencephalic brains at mid-neurogenesis (E14-15), when defects in proliferation and differentiation of cortical precursors can be easily assessed. Development of the mouse cortex follows a well-established pattern: radial precursors line the lateral ventricles and form the VZ, and can give rise to more radial precursors, neurons or intermediate neuronal progenitors (Fig. 1A). Above the VZ, intermediate neuronal progenitors divide away from the ventricular surface and populate the SVZ to eventually produce neurons (Englund et al., 2005). Newborn neurons migrate through the intermediate zone (IZ) to form the neuronal layers of the cortical plate (CP).

The morphology of *Fat1*$^{-/-}$ exencephalic brains was analyzed by staining coronal sections for the dorsal cortical precursor marker Pax6, the pan-neuronal marker βIII-tubulin, the intermediate neuronal progenitor marker Tbr2 (Eomes – Mouse Genome Informatics), the layer 2-4 neuronal marker Satb2 and the ventral interneuron marker Dlx2 (Fig. 2A; supplementary material Fig. S1E,F). This analysis revealed that the third ventricle is open in *Fat1*$^{-/-}$ exencephalic brains and that the thalamic region is expanded to the point of being displaced on top of the cortical

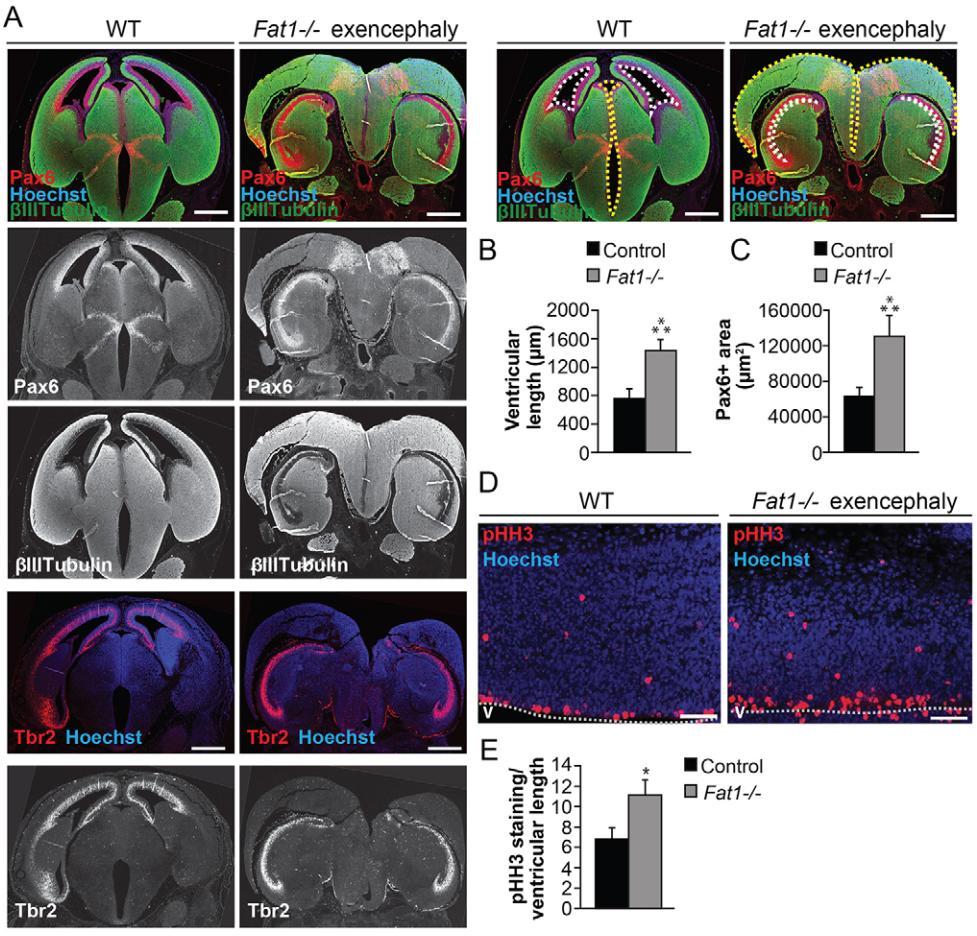

Fig. 2. *Fat1* exencephalic cortex exhibits elongated ventricles and increased proliferation. (A) Coronal section through E14.5 *Fat1*$^{-/-}$ exencephalic brain and control sibling stained for the dorsal cortical precursor marker Pax6 (red, top), the pan-neuronal marker βIII-tubulin (green), the intermediate neuronal progenitor marker Tbr2 (red, bottom) and with Hoechst (blue). Note that the third ventricle (yellow dotted line) is open in *Fat1*$^{-/-}$ exencephalic brains in the thalamic region (diencephalon) and is expanded dorsally above and over the cortex (telencephalon); the lateral ventricles of the cortex are delineated with white dotted lines. (B,C) Dorsal ventricular length (B) and Pax6^{+} area (C) measured from sections as in A. ***P<0.001; n=3 *Fat1*$^{-/-}$ exencephalic mutants and n=4 controls. (D) Coronal sections through E14.5 *Fat1*$^{-/-}$ exencephalic cortex and a control sibling stained for the mitosis marker phospho-histone H3 (pHH3, red) and with Hoechst (blue). V, ventricle (delineated with white dotted line). (E) Percentage of pHH3^{+} cells in the cortex, calculated per unit ventricle length, using images similar to D. *P<0.05; n=3 embryos each. Data are represented as mean±s.e.m. Scale bars: 500 μm in A; 20 μm in D.

Development (2015) 142, 2781-2791 doi:10.1242/dev.123539

hemispheres (Fig. 2A; supplementary material Fig. S1E,F). In contrast to the 'exposed' third ventricle of the thalamus, both the lateral ventricles of the cortex are present and appear closed. However, coronal cortical sections stained for Pax6 and Tbr2 revealed a dramatic lateral expansion of the VZ (Fig. 2A). Lateral ventricle length was quantified by measuring the length of the apical VZ lining the dorsal portion of the lateral ventricle, marked by Pax6, from different rostral-caudal coronal sections of *Fat1* mutants and control brains. This analysis revealed a ∼2-fold increase in ventricular length (Fig. 2B). This was accompanied by a ∼2-fold increase in the VZ area stained with the radial precursor marker Pax6 (Fig. 2C).

It has previously been shown that lateral expansion of the telencephalon is associated with aberrant proliferation of radial precursors (Chenn and Walsh, 2002). To directly test whether proliferation is altered in *Fat1* exencephalic mutants, we examined phospho-histone H3 (pHH3), a marker of mitosis (Fig. 2D). Immunostaining of cortical coronal sections for pHH3 revealed a ∼2-fold increase in the number of pHH3-positive cells per unit ventricular length in *Fat1* exencephalic cortices (Fig. 2E), indicating increased proliferation. We note that this analysis probably underestimates the increase in proliferation in *Fat1* mutants, since these exencephalic mutants also show increased ventricular length.

Fat1 regulates radial precursor maintenance independently of neural tube closure defects

Our analysis of *Fat1* mutant embryos suggested that Fat1 is involved in the control of radial precursor proliferation and maintenance, but these alterations could be secondary to the NTDs. To examine this possibility, we compared *Fat1* exencephalic mutants with *Vangl2* mutant embryos, which also exhibit NTDs. Vangl2 is a core PCP pathway component and its mutation leads to classical PCP defects, including an extreme NTD called craniorachischisis, in which the entire neural tube fails to close from the most anterior to posterior regions of the embryo (supplementary material Fig. S2A) (Kibar et al., 2001; Lake and Sokol, 2009). Coronal sections through E14-15 embryos showed that the lateral ventricles of *Vangl2* mutants are mostly similar to those of control siblings. In a few cases, *Vangl2* mutant ventricles showed some elongation, but never as dramatic as observed in *Fat1* mutants (data not shown). Moreover, pHH3 immunostaining of *Vangl2* mutants did not reveal any significant changes in the number of mitotic cells (supplementary material Fig. S2A,B). Thus, it is likely that little, if any, of the overproliferation observed in *Fat1* mutants can be attributed to NTDs.

Fat1 knockdown alters proliferation and maintenance of radial precursor cells

To determine the role of Fat1 in radial precursors in the absence of potential genetic compensation mechanisms in *Fat1* mutant mice, we used *in utero* electroporation to acutely knockdown Fat1 in the developing cortex (Fig. 3A). The efficiency of the Fat1 shRNA was first confirmed in cell culture, where it strongly decreased the expression of a tagged murine Fat1 (supplementary material Fig. S3A). Fat1 shRNA was electroporated with a nuclear EGFP expression vector into E13/14 cortices and embryos were harvested 3 days later. This approach transfects radial precursors that form the VZ (Gauthier et al., 2007). Many of these precursors differentiate into neurons over the subsequent 3 days, and migrate through the IZ to the CP (Fig. 3A). Analysis of coronal cortical sections showed that Fat1 knockdown caused mislocalization of EGFP-positive cells, with more cells in the SVZ and IZ compared with control electroporated brains (Fig. 3B,C). We examined whether this change in cell localization reflected a change in precursor number and proliferation by immunostaining similar sections for the radial precursor marker Pax6 and the proliferation marker Ki67 (Fig. 3D,G). Knockdown of Fat1 caused a significant increase in Pax6-positive radial precursors, accompanied by a modest but significant increase in proliferation (Fig. 3E,H). In addition, significantly more of the Pax6-positive cells were localized in the IZ, with correspondingly fewer in the VZ, in Fat1 knockdown brains (Fig. 3F). This coincided with an increase in the proportion of proliferating radial precursors, as monitored by double labeling for Pax6 and Ki67 (Fig. 3I; supplementary material Fig. S3B). Intriguingly, the proliferating radial precursors were localized to the IZ (Fig. 3J; supplementary material Fig. S3B). In contrast to radial precursors, the proportion of Tbr2-positive intermediate neuronal progenitors was unchanged upon Fat1 knockdown (Fig. 3K,L). However, a significant percentage of these coexpressed Pax6 and Tbr2 (Fig. 3M; supplementary material Fig. S3C). Thus, Fat1 knockdown leads to an increase in proliferating radial precursors and an increase in the proportion of intermediate progenitors that still express Pax6.

To determine whether this increase in radial precursor maintenance was accompanied by a decrease in neuronal differentiation, we stained similar sections for the pan-neuronal marker βIII-tubulin and the neuronal layer 2-4 marker Satb2, which marks the majority of neurons that are born during the time frame of our *in utero* electroporation experiments (Tsui et al., 2013) (Fig. 3N; supplementary material Fig. S3D,E). Knockdown of Fat1 caused a significant reduction in the proportion of neurons positive for EGFP, βIII-tubulin and Satb2 (Fig. 3O,Q) and a mislocalization of these neurons below the CP (Fig. 3P,R; supplementary material Fig. S3D,E). Thus, Fat1 knockdown alters radial precursor proliferation, differentiation and neuronal migration.

Loss of Fat4 interacts genetically with loss of Fat1 to increase exencephaly penetrance

Interestingly, previous work showed exencephaly in $Fat1^{-/-}$ embryos only when *Fat4* was also deleted (Saburi et al., 2012). This difference is likely to be due to the different genetic backgrounds of the mouse strains used to breed our *Fat1* and *Fat4* mutant mice. Indeed, crossing $Fat1^{+/-}$; $Fat4^{+/-}$ mice onto a number of different mice strains confirmed this hypothesis (supplementary material Fig. S4A). We found that the exencephaly phenotype is primarily dependent on loss of both *Fat1* alleles, with enhancement from additional loss of *Fat4* alleles occurring in a few genetic backgrounds. In outbred CD-1 mice, for example, deletion of *Fat1* alone results in exencephaly in ∼20-30% of progeny, with no effects from additional loss of *Fat4*, whereas the frequency of the phenotype increased from 20% (1/5) to 57% (4/7) upon loss of one allele of *Fat4* in a mixed 129/B6 background (supplementary material Fig. S4A). Thus, depending on the genetic strain of the mice, Fat4 and other unknown genetic modifiers play redundant, compensatory roles with regard to the cranial NTD caused by loss of Fat1.

We analyzed $Fat1^{-/-}$; $Fat4^{-/-}$ or $Fat1^{-/-}$; $Fat4^{+/-}$ exencephalic embryos, in the mixed 129/B6 or CD-1 genetic background, by immunostaining of E14-15 coronal cortical sections. We henceforth refer to these as *Fat1-Fat4* mutants. *Fat1-Fat4* mutants have similar brain morphology to *Fat1* mutants (supplementary material Fig. S4B,C; data not shown). Cortical ventricle length was measured by immunostaining similar sections for the cortical

Development (2015) 142, 2781-2791 doi:10.1242/dev.123539

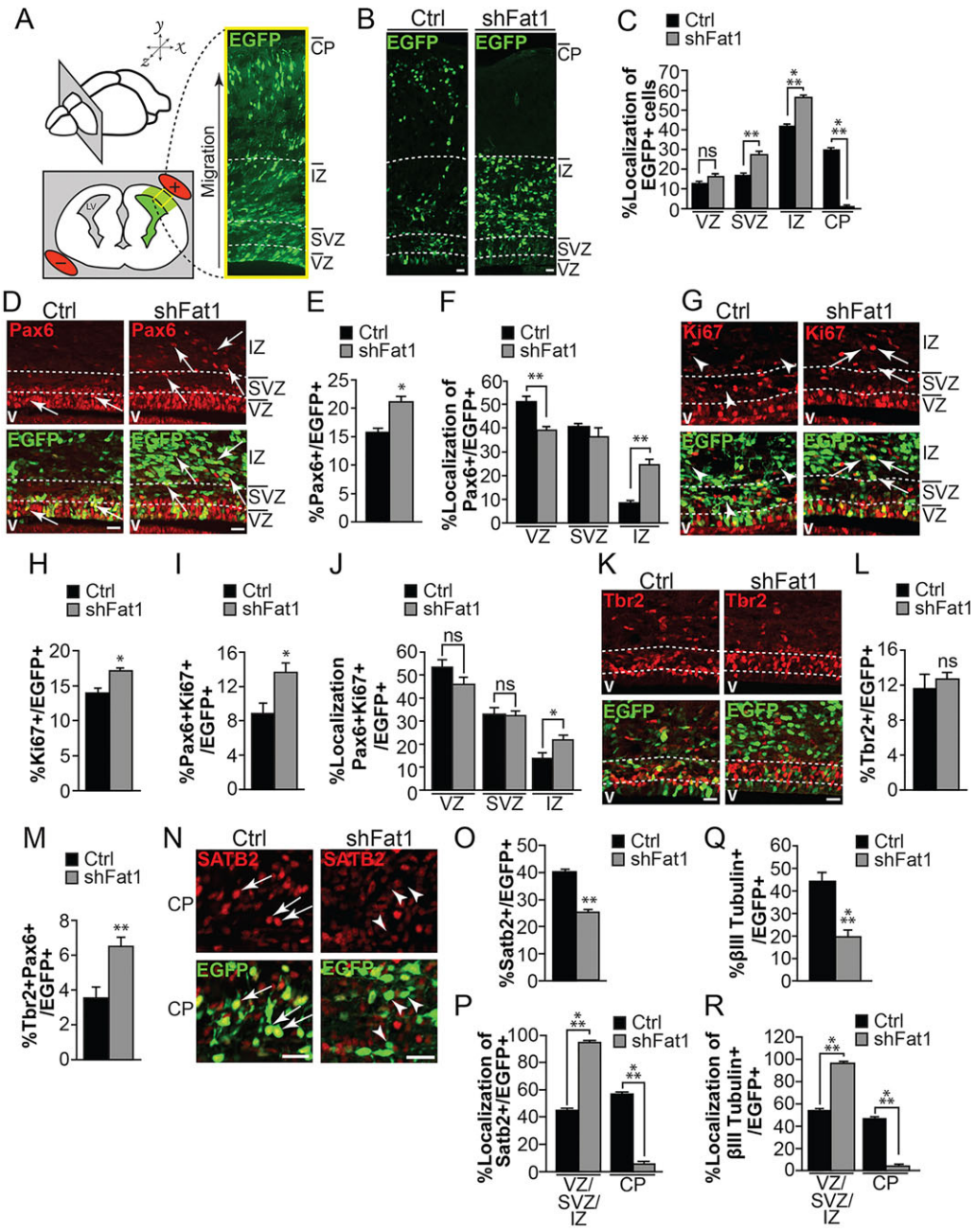

Fig. 3. Fat1 knockdown promotes radial glial precursor proliferation. (A) Schematic of the *in utero* electroporation technique. (B-R) Murine cortices were electroporated at E13.5 with a nuclear EGFP expression plasmid and Fat1 shRNA (shFat1) or a scrambled shRNA (Ctrl) plasmid, and analyzed 3 days later at E16/17. (B) Fluorescence confocal micrographs of E16.5 cortex stained for EGFP (green). (C) Quantification of sections as in B for the percentage localization of EGFP$^+$ cells (*n*=3 embryos each). (D) Confocal fluorescence micrographs of VZ/SVZ/IZ from coronal sections through E16.5 cortex immunostained for Pax6 (red) and EGFP (green); bottom panels show merge. (E,F) Quantification of sections as in D for the proportion of Pax6$^+$, EGFP$^+$ cells per section (E; *n*=3 embryos each) and relative localization in the VZ, SVZ or IZ (F; *n*=3 embryos each). (G) Confocal fluorescence micrographs of VZ/SVZ/IZ from coronal E16.5 cortical sections immunostained for Ki67 (red) and EGFP (green); bottom panels show merge. (H) Quantification of sections as in G for proportion of Ki67$^+$, EGFP$^+$ cells per section (*n*=3 embryos each). (I,J) Quantification of sections as in supplementary material Fig. S3B for the proportion of Pax6$^+$, Ki67$^+$, EGFP$^+$ triple-labeled cells per section (I; *n*=3 embryos each) and relative localization in the VZ, SVZ or IZ (J; *n*=3 embryos each). (K) Fluorescence confocal micrographs of VZ/SVZ/IZ from coronal E16.5 cortical sections stained for Tbr2 (red) and EGFP (green); bottom panels show merge. (L) Quantification of sections as in K for the proportion of Tbr2$^+$, EGFP$^+$ cells per section (*n*=3 embryos each). (M) Quantification of sections as in supplementary material Fig. S3C for the proportion of Pax6$^+$, Tbr2$^+$, EGFP$^+$ triple-labeled cells per section (*n*=3 embryos each). (N) Fluorescence confocal micrographs of CP from coronal E16.5 cortical sections immunostained for Satb2 (red) and EGFP (green); lower panels show merge. (O,P) Quantification of sections as in N and supplementary material Fig. S3D for the proportion of Satb2$^+$, EGFP$^+$ cells per section (O; *n*=3 embryos each) and relative localization in the VZ/SVZ/IZ versus CP (P; *n*=3 embryos each). (Q,R) Quantification of sections as in supplementary material Fig. S3E for the proportion of βIII-tubulin$^+$, EGFP$^+$ cells per section (Q; *n*=3 embryos each) and the relative localization in the VZ/SVZ/IZ versus CP (R; *n*=3 embryos each). Arrowheads indicate EGFP$^+$ cells negative for the respective marker and arrows indicate double-labeled cells. **P*<0.05, ***P*<0.01, ****P*<0.001; ns, not significant; error bars denote s.e.m. Scale bars: 20 µm.

Development (2015) 142, 2781-2791 doi:10.1242/dev.123539

precursor markers Sox2 and Pax6, and quantifying the length of the apical VZ lining the lateral ventricle (supplementary material Fig. S4B,C). This analysis showed that *Fat1-Fat4* exencephalic lateral ventricles are twice as long as those of control littermates (supplementary material Fig. S4D). Moreover, similar to what we observed in *Fat1* mutant exencephalic cortex, a ~3-fold increase in pHH3 staining was measured in *Fat1-Fat4* mutant cortices (supplementary material Fig. S4E,F).

Loss of Fat cadherins leads to a decrease in cell cycle exit of radial precursors

To further analyze cortical precursor proliferation, we injected pregnant *Fat1-Fat4* mutant mice at E13.5 with BrdU, a thymidine analog that incorporates into the DNA of cells undergoing S phase. Embryos were harvested at E14.5 and immunostained for BrdU and Ki67 (Fig. 4A). Analysis of BrdU-positive, Ki67-negative cells revealed that the proportion of cells that exited the cell cycle within 24 h following the BrdU injection was significantly decreased in *Fat1-Fat4* exencephalic cortices, indicating that more cells remained in the cell cycle (Fig. 4B). To address which cell type is affected, sections were stained for BrdU and the radial precursor marker Sox2 (Fig. 4C). In *Fat1-Fat4* exencephalic mutants, there is a significant increase in the proportion of BrdU-labeled cells that are Sox2-positive precursors (Fig. 4D). Co-staining of BrdU with the intermediate neuronal progenitor marker Tbr2 revealed no change in this population of progenitors, suggesting that Fat1 specifically affects proliferation of radial precursors (Fig. 4E,F). Together, these data suggest that the exencephaly observed upon loss of *Fat1-Fat4* is due, in part, to an increase in cortical radial precursor proliferation, leading to a laterally expanded cortex.

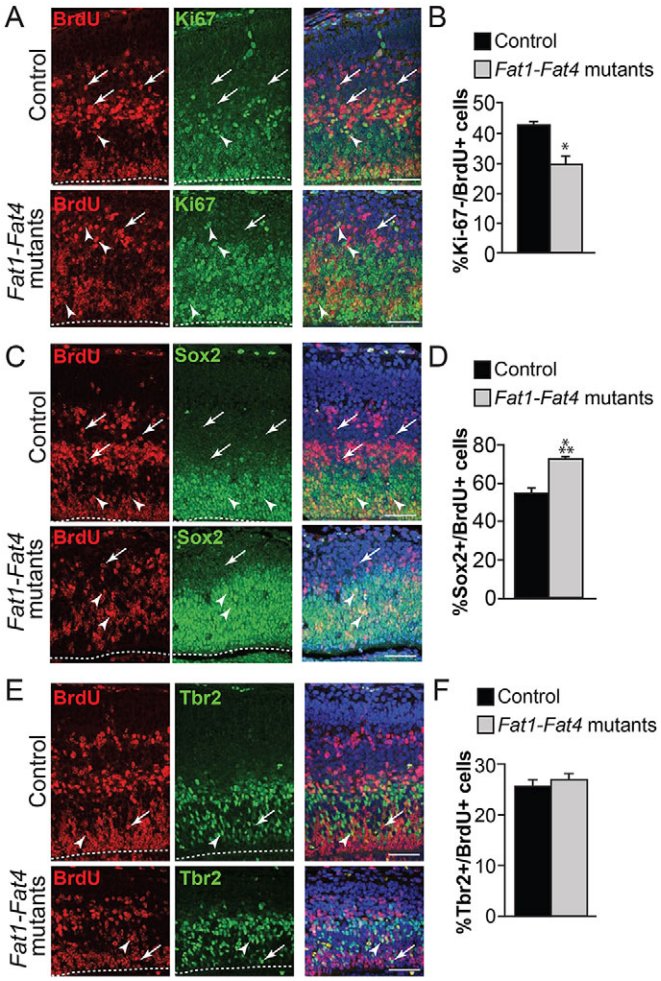

Fig. 4. *Fat1-Fat4* mutant cortices display enhanced radial precursor proliferation and delayed cell cycle exit. E13.5 *Fat1-Fat4* mutant embryos and control siblings were labeled with BrdU and harvested after 24 h. (A,C,E) Coronal sections through E14.5 dorsal cortex stained for BrdU (red) and Ki67 (A), Sox2 (C) and Tbr2 (E) (green); right panel shows merge with Hoechst (blue). Arrowheads point to examples of double-labeled cells ($BrdU^+$ and $Ki67^+$, $Sox2^+$ or $Tbr2^+$) and arrows to single-labeled $BrdU^+$ cells. Scale bars: 50 µm. (B,D,F) Quantification of the percentage of $Ki67^-$, $BrdU^+$ (B), $Sox2^+$, $BrdU^+$ (D) and $Tbr2^+$, $BrdU^+$ (F) over total $BrdU^+$ cells shows reduced cell cycle exit in *Fat1-Fat4* mutants. **P*<0.05, ****P*<0.001; *n*=3 embryos each; data are mean±s.e.m.

Fat1 and Fat4 knockdown have additive effects on radial precursor maintenance

To examine whether, as suggested by the knockout data, Fat1 and Fat4 interact genetically to regulate radial precursor proliferation, we performed *in utero* electroporations with Fat4 shRNA. Analysis of cortical sections 3 days post-electroporation showed that, as observed with Fat1 knockdown, Fat4 knockdown leads to the mislocalization of EGFP-positive cells (supplementary material Fig. S5A,B) and an increase in Pax6-positive radial precursors (supplementary material Fig. S5C,D), with a greater number in the IZ and fewer in the VZ compared with controls (supplementary material Fig. S5E). This was accompanied by a mislocalization and decreased number of Satb2-positive neurons (supplementary material Fig. S3D and S5F-H). The proliferation of EGFP-positive cells was not significantly altered, as assessed by Ki67 staining (supplementary material Fig. S5I,J).

To determine whether Fat1 and Fat4 interact genetically to regulate cortical development, we performed concomitant knockdown of Fat1 and Fat4. Analysis of cortical sections 3 days following *in utero* electroporation of both Fat1 and Fat4 shRNAs revealed a mislocalization of EGFP-positive cells that was similar to that seen with single knockdowns (Fig. 5A,B). Immunostaining for Pax6 showed that knockdown of both Fat1 and Fat4 caused an increase in the proportion of EGFP-positive, Pax6-positive radial precursors (Fig. 5C,D), which were also mislocalized, with a greater number of these cells in the IZ than the VZ compared with controls (Fig. 5E). This increase was greater than that observed upon independent knockdown of either Fat1 or Fat4 alone (shFat1 or shFat4 versus shFat1-4, $P<0.05$; Ctrl versus shFat1-4, $P<0.001$). The increase in radial precursors was accompanied by an increase in proliferating, EGFP-positive, Ki67-positive cells (Fig. 5F,G), which was also significantly greater than that seen upon knockdown of Fat1 or Fat4 individually (shFat4 versus shFat1-4, $P<0.01$; shFat1 versus shFat1-4, $P<0.05$; Ctrl versus shFat1-4, $P<0.001$). Coincident Fat1 and Fat4 knockdown also decreased the proportion of EGFP-positive, Satb2-positive neurons, with a greater proportion of these neurons found below the CP (Fig. 5H-J). Thus, Fat1 and Fat4 interact genetically to regulate the proliferation and maintenance of radial precursors.

Fat1 and Fat4 regulate the actin cytoskeleton and apical constriction of radial glial precursors

The apical domain of radial precursors is composed of endfeet with adherens junctions that span the lateral ventricles. Apical junctions have been shown to play a role in symmetric versus asymmetric divisions in radial precursors (reviewed by Fietz and Huttner, 2011; Shitamukai and Matsuzaki, 2012). We therefore

Development (2015) 142, 2781-2791 doi:10.1242/dev.123539

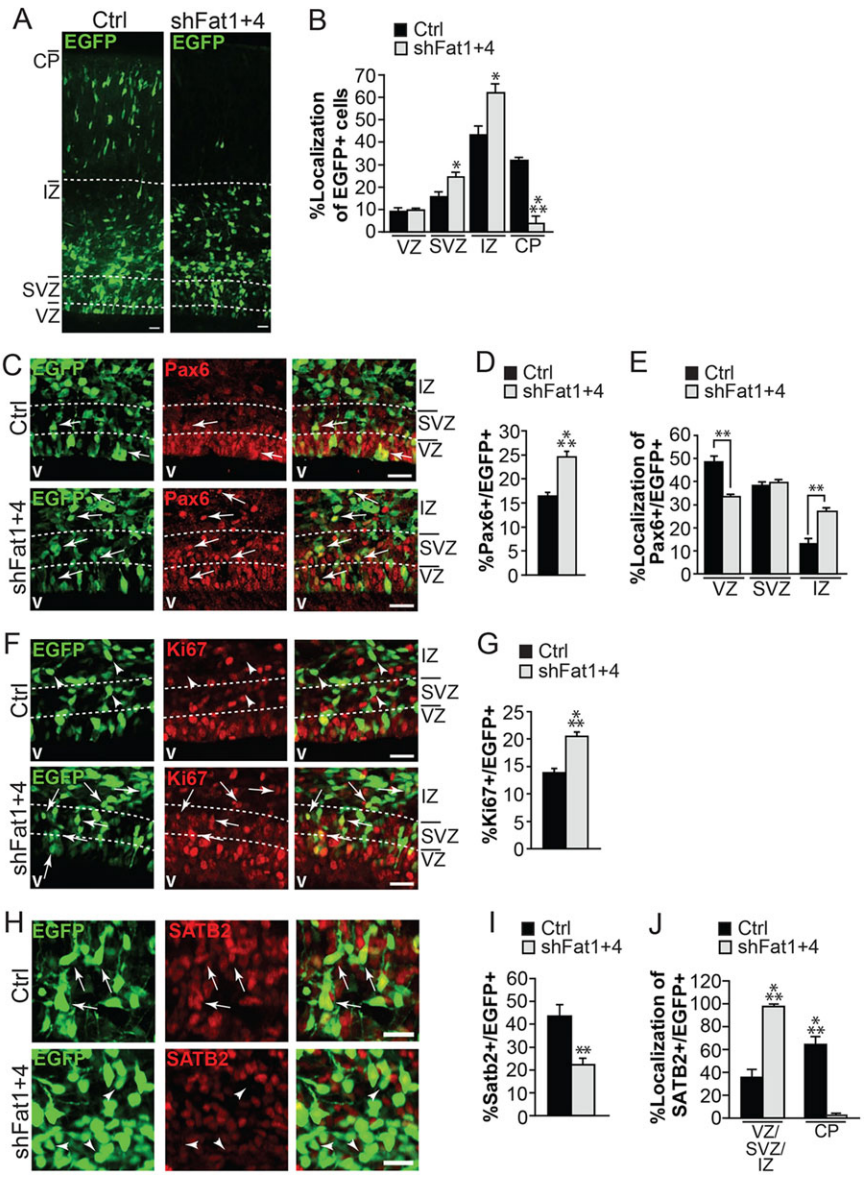

Fig. 5. Fat1 and Fat4 have additive effects on radial glial precursor proliferation. (A-J) Murine cortices were electroporated with a nuclear EGFP expression plasmid and a control shRNA (Ctrl) or combined Fat1 shRNA and Fat4 shRNA at E13.5, and analyzed 3 days later at E16/17. (A) Confocal fluorescence micrographs of E16.5 coronal cortical sections stained for EGFP (green). (B) Quantification of sections as in A for the relative localization of EGFP$^+$ cells (n=3 embryos each). (C) Confocal fluorescence micrographs of the VZ/SVZ/IZ of coronal cortical sections immunostained for EGFP (green) and Pax6 (red); right panels show merge. (D,E) Quantification of sections as in C for the proportion of Pax6$^+$, EGFP$^+$ cells per section (D; n=3 embryos each) and the relative localization in the VZ, SVZ or IZ (E; n=3 embryos each). (F) Confocal fluorescence micrographs of the VZ/SVZ/IZ of sections stained for EGFP (green) and Ki67 (red); right panels show merge. (G) Quantification of sections as in F for the proportion of EGFP$^+$ cells that are Ki67$^+$ (n=3 embryos each). (H) Confocal micrographs of the CP stained for EGFP (green) and Satb2 (red); right panels show merge. (I,J) Quantification of sections as in H for the proportion of EGFP$^+$ cells that are Satb2$^+$ (I; n=3 embryos each) and relative localization in VZ/SVZ/IZ versus CP (J; n=3 embryos each). Dotted lines demarcate cortical regions. Arrowheads indicate EGFP$^+$ cells negative for the respective marker and arrows indicate double-labeled cells. *P<0.01, **P<0.01, ***P<0.001; error bars denote s.e.m. Scale bars: 20 µm.

analyzed the junctional proteins ZO-1 (Tjp1), Par3 (Pard3), Mupp1 (Mpdz), Pals1 (Mpp5) and β-catenin in cortical sections of *Fat1* and *Fat1-Fat4* mutant exencephalic embryos (Fig. 6A; supplementary material Fig. S6A; data not shown). Immunostaining for these proteins showed no apparent change in any of these apical markers, indicating that apical junctions are still present in the exencephalic brains.

Apical junctions of radial precursors are connected to a rich actin network that maintains normal apical constriction at the ventricular surface. Since Fat1 has been linked to F-actin regulation (Moeller et al., 2004; Tanoue and Takeichi, 2004), we analyzed the integrity of the apical actin network of these cells by staining sections with Rhodamine-phalloidin. Interestingly, we observed a decrease in F-actin staining at the apical junctions of *Fat1-Fat4* exencephalic mutants (Fig. 6B). Quantification of phalloidin intensity at apical cell junctions revealed a 20% decrease in actin accumulation in *Fat1-Fat4* exencephalic mutants compared with control siblings (Fig. 6C).

To analyze the morphology of radial precursor apical endfeet and check for associated apical constriction defects, we analyzed thick cortical coronal sections (10 µm). Sections were immunostained for ZO-1 and/or Par3 to delineate the apical domain of radial precursors, and z-stack confocal images were reconstructed to obtain an orthogonal view of the apical surface (Fig. 6A). In *Fat1*$^{-/-}$ and *Fat1-Fat4* exencephalic cortices, the apical surface area of radial precursors increased by ∼20% compared with control siblings, suggesting that Fat1 regulates the apical constriction of radial precursors, possibly through regulating actin abundance at the apical junctions (Fig. 6D,E; supplementary material Fig. S6B,D).

To test whether this apical expansion phenotype is specific to loss of *Fat1*, and not a secondary defect due to NTDs, we analyzed *Vangl2*$^{-/-}$ embryos, which have a severe NTD (supplementary material Fig. S6C). *Vangl2* mutants showed no increase in the apical surface area of cortical precursors compared with control littermates (supplementary material Fig. S6D). This indicates that the apical constriction defect seen in *Fat1* and *Fat1-Fat4* exencephalic mutants is not simply a consequence of cranial NTDs but is specifically caused by mutations in Fat cadherins.

Development (2015) 142, 2781-2791 doi:10.1242/dev.123539

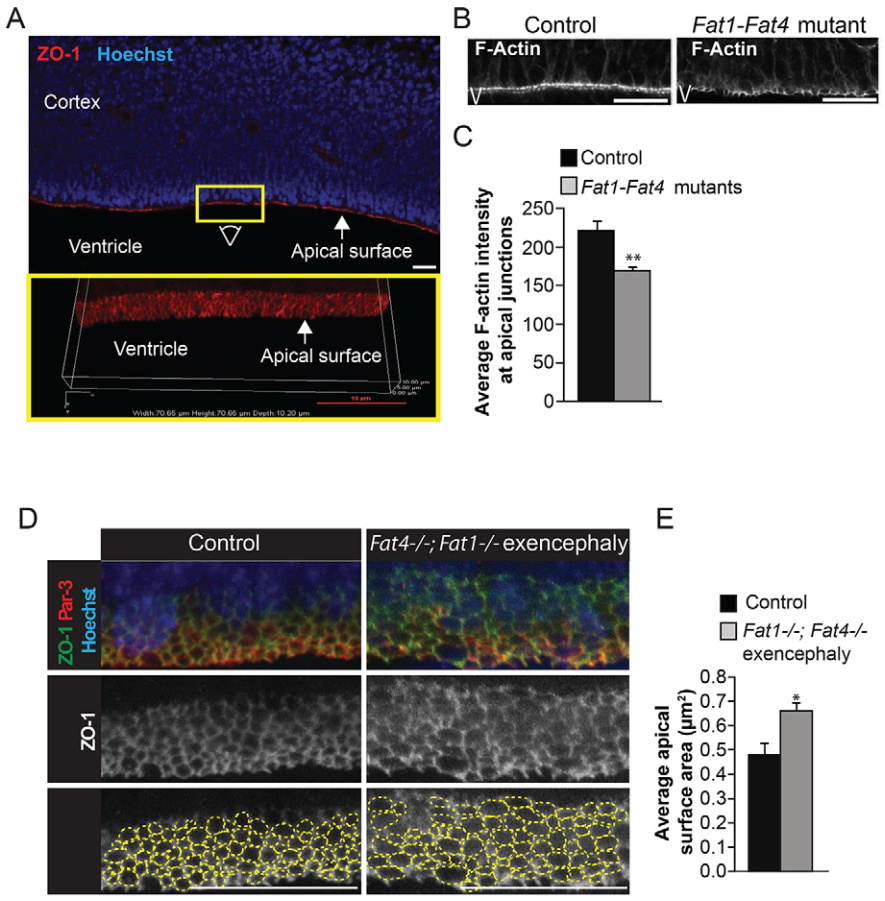

Fig. 6. *Fat1-Fat4* mutant radial glial precursors have apical constriction defects. (A) ZO-1 staining of thick coronal sections (10 µm). Beneath is a reconstruction of the apical surface area from *z*-stack confocal images. (B) Confocal fluorescence micrographs of the ventricular domain of cortical sections from E14.5 *Fat1-Fat4* mutants and control sibling. Rhodamine-phalloidin was used to visualize F-actin. (C) Quantification of F-actin intensity from images as in B, showing a decrease in F-actin accumulation in *Fat1-Fat4* mutants. $^{**}P<0.01$; $n=4$ controls and $n=3$ *Fat1-Fat4* mutants, at least 100 junctions were measured for each. (D) Reconstruction of radial precursor apical surface in $Fat1^{-/-}; Fat4^{-/-}$ E14.5 cortex and control sibling stained for ZO-1 (green), Par3 (red) and Hoechst (blue). (E) Quantification of apical surface area. $^{*}P<0.05$; $n=7$ controls and $n=4$ *Fat1-Fat4* mutants, at least 100 cells were measured for each on at least two different stacks images. Scale bars: 10 µm in A,D; 20 µm in B. Data are mean±s.e.m.

Fat1 and Fat4 bind distinct sets of junctional and cytoskeletal proteins

The additive effects we observed with loss of *Fat1* and *Fat4 in vivo*, and with Fat1 and Fat4 knockdown *in utero*, suggest that Fat4 and Fat1 interact genetically to regulate cortical precursor maintenance and neural tube closure. All mammalian Fat homologs have very similar extracellular domains; however, their intracellular domains are more divergent, suggesting that they control different intracellular pathways. Alignment of the Fat1 and Fat4 intracellular domains, in particular, revealed only 29% sequence identity, suggesting the additive effects we observed are not solely due to redundancy.

To determine which proteins might mediate the functions of Fat1 and Fat4 in controlling apical constriction and proliferation, we used affinity purification coupled to mass spectrometry to determine the interactome of Fat1 and Fat4. To specifically look for intracellular targets and because Fat cadherins are huge proteins with enormous extracellular domains (>400 kDa), we used Flag-tagged deletion constructs containing the intracellular domains of both proteins (Fat1-ICD-Flag and Fat4-ICD-Flag). Fusion proteins were stably expressed in HEK293 cells, affinity purified using anti-Flag-conjugated beads and subjected to mass spectrometry to identify associated polypeptides. For both Fat1 and Fat4 we focused on a list of potential interactors identified with a total of at least 20 high-confidence peptides (supplementary material Fig. S7).

Interestingly, Fat1 and Fat4 interactomes shared very little overlap, suggesting that they have distinct sets of intracellular partners. Some of these proteins are already known to bind Fat1 (Mena, Vasp and Homer) or Fat4 (Lix1l, Mupp1), validating the biological significance of our results (Moeller et al., 2004; Tanoue and Takeichi, 2004; Ishiuchi et al., 2009). The finding that Fat1 binds Mena and Vasp is exciting, as loss of Mena/Vasp causes NTDs (Menzies et al., 2004), providing a potential mechanism for neural tube defects in *Fat1* mutants.

We confirmed these biochemical interactions using immunoprecipitation followed by western blot. This analysis showed that Fat1-ICD-Flag binds strongly to endogenous Mena and Vasp (Fig. 7A; data not shown). We also immunoblotted Fat1-ICD-

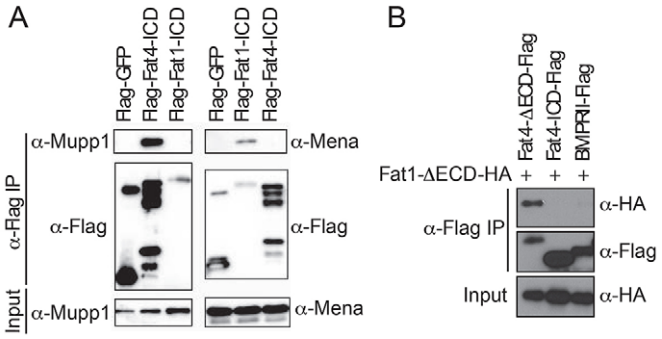

Fig. 7. Fat1 and Fat4 form heterodimers and have different binding partners. (A) HEK293 cells stably expressing Fat1-ICD-Flag and Fat4-ICD-Flag constructs, or a control (GFP-Flag), were subjected to Flag immunoprecipitation followed by western blot with antibodies against Mena and Flag, as indicated. (B) HEK293 cells were co-transfected with an HA-tagged Fat1 construct missing most of its extracellular domain (Fat1-ΔECD-HA), together with Flag-tagged Fat4 constructs (Fat4-ΔECD-Flag or Fat4-ICD-Flag) or BMPRII as control. Flag immunoprecipitates were subject to western blot with antibodies against HA and Flag, as indicated.

Development (2015) 142, 2781-2791 doi:10.1242/dev.123539

Flag immunoprecipitates with antibodies to the Fat4 ICD interactor Mupp1. Importantly, Fat1-ICD-Flag does not bind Mupp1, nor is it found in the Fat1 interactome. This analysis confirmed the specificity of our Fat1 and Fat4 interactomes. We also confirmed a strong interaction between Fat4-ICD-Flag and the apical junction protein Mupp1 (Fig. 7A).

Fat4-ICD-Flag immunoprecipitates were also subjected to western blot to test the interaction with a newly identified Fat4 interactor, Par3. Immunoblotting for Fat4 ICD immunoprecipitates with antibodies to endogenous Par3 confirmed the interaction with Fat4 (data not shown). We also immunoblotted Fat4-ICD-Flag immunoprecipitates with antibodies to Mena (Fig. 7A) and found that Fat4-ICD-Flag does not bind to Mena. Together, these data indicate that Fat1 and Fat4 bind a different set of downstream effectors and identify novel interactors for both the Fat1 and Fat4 ICDs.

Fat1 and Fat4 can form cis-heterodimers

The identification of the unique interactomes of Fat1 and Fat4 could help explain the divergent roles of Fat1 and Fat4 but does not explain their common functions. In *Drosophila*, Fat forms cis-homodimers (Feng and Irvine, 2009; Sopko et al., 2009). We examined whether Fat1 and Fat4 also form cis-heterodimers, potentially explaining their common functions and genetic interactions. We transfected HEK293 cells with tagged Fat1 and Fat4 constructs lacking the majority of their extracellular domains but containing the transmembrane and cytoplasmic domains (Fat1-ΔECD-HA and Fat4-ΔECD-Flag). Lysates were immunoprecipitated with a Flag antibody, and western blots were performed with an HA antibody to determine if Fat1 co-immunoprecipitated with Fat4 (Fig. 7B). Importantly, we found that Fat1-ΔECD-HA binds strongly to Fat4-ΔECD-Flag (Fig. 7B), but not to another transmembrane protein used as a negative control. We also found that Fat1-ΔECD-HA does not co-immunoprecipitate with a truncated Fat4 composed solely of the ICD, without the transmembrane domain (Fat4-ICD-Flag), suggesting that Fat4 interacts with Fat1 via its transmembrane domain. Thus, Fat1 and Fat4 can bind to one another, forming cis-heterodimers that could bring together diverse protein partners to regulate neural progenitor proliferation, apical constriction and neural tube closure.

DISCUSSION

Here, we provide the first characterization of Fat1 function in neural development. We demonstrate that the atypical cadherin Fat1 is crucial for cranial neural tube closure and proliferation of cortical precursors. We show that Fat1 regulates apical constriction and actin accumulation of radial precursors in the developing mouse brain. We also demonstrate that Fat4 can interact with Fat1, and shares some functions with Fat1 during brain development. However, we find that the interactomes of Fat1 and Fat4 are distinctly different. We propose a model in which Fat1 and Fat4 interact at subapical junctions, where they form complexes with actin regulators and apical junction proteins, respectively. We suggest this is important for maintaining radial precursor apical constriction and for regulating the balance between self-renewal and asymmetric neurogenic divisions.

Through our unbiased interactome analysis of Fat1, we show that Fat1 specifically forms a complex with several actin-regulating proteins and we observe a decrease in actin accumulation in *Fat1* mutant radial precursors. Interestingly, it has previously been shown that deletion of two actin-regulating interactors, Mena and Vasp, leads to the same cranial neural tube defect as we observe in *Fat1* mutants (Menzies et al., 2004). These data suggest that Fat1 regulates neural tube closure by regulating the activity of the Mena/Vasp complex. This also fits with previous data showing that Fat1 regulates actin dynamics and actin-dependent cell motility in cell culture through Mena/Vasp (Moeller et al., 2004). Observation of Mena/Vasp localization through immunostaining did not reveal any changes in the accumulation or localization of these proteins, suggesting that Fat1 is not necessary to simply anchor these actin-regulating proteins at the apical junctions. We speculate that Fat1-Fat4 binding promotes cross-talk between actin-regulating and junctional proteins, leading to the constriction of apical junctions and suppression of growth.

Interestingly, a recent study in zebrafish retina revealed that an increase in the apical surface area of neuroepithelial cells, through inhibition of Shroom3 and Llgl1, could affect neurogenesis (Clark et al., 2012). Moreover, mouse *Shroom* mutants exhibit NTDs similar to those we show for *Fat1* (Hildebrand and Soriano, 1999). Thus, apical constriction might be an important mechanism to regulate the proliferation of various neuroepithelia.

We believe that the radial precursor maintenance and overproliferation phenotype observed in *Fat1* and *Fat1-Fat4* exencephalic mutants is the direct result of *Fat1* and *Fat4* deletions and not a secondary defect due to abnormal neural tube closure. First, Fat1 and Fat4 are both expressed at mid-neurogenesis in the frontal cortex, specifically in radial precursors, suggesting they play a role in brain development after neural tube closure (our data; Ishiuchi et al., 2009). Second, acute loss of Fat1 and/or Fat4 in radial precursors by *in utero* electroporation resulted in enhanced radial glial precursor proliferation that occurs without neural tube closure defects. Third, overproliferation was not observed in the core PCP pathway *Vangl2* mutant, which also has severe NTDs.

Recent studies suggest a role for the Yorkie homolog Yap (Yap1) in controlling neural progenitor maintenance downstream of Fat4 (Van Hateren et al., 2011; Cappello et al., 2013). In the developing cortex, Yap is expressed in radial precursors and not in differentiated neurons (Cappello et al., 2013). Immunostaining of Yap in *Fat4* and/or *Fat1* mutants revealed an expansion of Yap-positive cells that follows the expansion of radial precursors (data not shown). However, we did not observe any changes in Yap localization, nuclear:cytoplasmic ratio, or accumulation that could be indicative of Yap inhibition by the Hippo pathway. Similarly, western blot analyses of embryonic cortex extracts revealed no changes in the phosphorylated inactive forms of Yap or its homolog Taz (Wwtr1 – Mouse Genome Informatics) (data not shown). These data suggest that changes in Yap activity are not responsible for the overproliferation seen in $Fat1^{-/-}$; $Fat4^{-/-}$ mutants.

Radial precursors have a unique morphology, with apical domains that span the lateral ventricles and long basal processes that extend to the pia matter of the cortex. Cell divisions occur at the apical surface of the ventricles, and it is believed that apical junctions and cell division asymmetry play a role in regulating self-renewal versus neurogenic divisions (Bultje et al., 2009; Marthiens and ffrench-Constant, 2009). Our data indicate that Fat cadherins are important in controlling the balance between self-renewal and neurogenic division and do not change the ratio of intermediate neuronal progenitors.

Interestingly, we observe the presence of basally located Pax6-positive radial precursors upon Fat1 and Fat4 knockdown, suggesting that Fat1-4 are involved in anchoring radial precursors at the apical ventricular surface. However, we also see an increase in apical mitosis, suggesting that apical anchoring is not the sole

Development (2015) 142, 2781-2791 doi:10.1242/dev.123539

means by which they regulate neuronal radial precursor proliferation.

We note that our *in utero* electroporation studies also suggest that there are defects in radial migration, which might be linked to defects in the cytoskeleton. More work is needed to determine the basis of these potential migration defects and whether these basally localized Pax6-positive radial precursors could be outer radial glial cells (oRG) (Wang et al., 2011).

Loss of Fat1 and Fat1-Fat4 leads to reduced apical constriction and decreased actin accumulation at cell junctions. Fat cadherins bind both junctional and cytoskeletal proteins, which could explain the reduced apical constriction. We favor the hypothesis that defects in apical constriction contribute to radial precursor overproliferation. Although the link between apical constriction and proliferation in the control of neuroepithelium remains to be elucidated, we speculate that enlargement of apical surfaces increases cell exposure to extracellular proliferation cues from the ventricle. Alternatively, it is possible that lack of junctional constrictions might perturb the asymmetric distribution of cellular components during mitosis and create a bias toward symmetrical divisions. More studies will be needed to elucidate these mechanisms.

We note that only a subset of *Fat1*$^{-/-}$; *Fat4*$^{-/-}$ double-mutant embryos show exencephaly and neural progenitor proliferation defects (from 20-57%, depending on the genetic background). We do not see any defects in apical surface area, progenitor proliferation or neural tube closure in non-exencephalic embryos (*Fat1*$^{-/-}$, *Fat4*$^{-/-}$ or *Fat1*$^{-/-}$; *Fat4*$^{-/-}$; supplementary material Fig. S8; data not shown). Since we have shown proliferation defects in *in utero* knockdown experiments and because other neural tube defects do not cause the constriction or proliferation defects, we do not believe that exencephaly causes radial precursor overproliferation or changes in apical junctions. Instead, we think that, in a subset of Fat mutant embryos, the weakening of junctions leads to variable apical constriction defects that cause overproliferation and neural tube closure defects.

Fat1 and Fat4 are relatively divergent, as indicated by the low sequence identity of their ICDs, and this is consistent with our unbiased identification of completely different interactomes for the two proteins. However, our genetic data show that Fat4 and Fat1 share functions in neural tube closure and proliferation control, and our biochemical analysis suggests Fat1 and Fat4 interact in cis. We propose that Fat1 and Fat4 binding regulates radial precursor development. Because the Fat4 interactome includes junctional proteins (Par3, Mupp1), the two bound cadherins are in an ideal position to regulate crosstalk between apical junctions and actin dynamics. Such cooperation is needed throughout development, and especially in brain development where the neuroepithelium has to go through drastic morphological changes to form the complex layered neural cortex, and to titer self-renewal with complex differentiation.

MATERIALS AND METHODS

Mouse lines

Mouse lines are described in the supplementary Methods. Husbandry and ethical handling of mice were conducted according to guidelines approved by the Canadian Council on Animal Care.

Histological and immunological analyses

Embryonic samples from timed matings were fixed in 4% paraformaldehyde overnight at 4°C, serially dehydrated and embedded in paraffin. For immunofluorescent analysis, paraffin sections were dewaxed and rehydrated via an ethanol series. Antigen retrieval was performed by boiling the sections for 20 min in Antigen Unmasking Solution (H-3300, Vector Laboratories). After blocking for 1 h in 3% BSA, 10% goat serum and 0.1% Tween 20 in PBS, sections were incubated overnight with primary antibodies diluted in 3% BSA, 3% goat serum, 0.1% Tween 20 in PBS. For details of antibodies, see the supplementary Methods.

Cryosections were prepared as described (Barnabé-Heider et al., 2005). Rhodamine-phalloidin (1:400; Invitrogen) was incubated for 1 h on cryosections.

Fluorescent images were taken with a Nikon C1 Plus Digital Eclipse confocal microscope. For apical surface reconstruction, 0.15 µm *z*-stack confocal sections were taken and 3D reconstruction obtained with NIS-Elements software (Nikon).

β-galactosidase staining

For staining of coronal sections of embryonic brain, a protocol similar to that of Nagy et al. (2007) was followed with minor modifications, as detailed in the supplementary Methods.

In situ hybridization

Digoxigenin-UTP-labeled *Fat1* riboprobes were generated and samples processed according to standard protocols (Komatsu et al., 2014).

BrdU incorporation

Analysis of cell cycle exit by BrdU incorporation is described in the supplementary Methods.

In utero electroporation and quantification

In utero electroporation was performed as described (Gauthier et al., 2007) with E13/14 CD-1 mice, injecting a 1:3 ratio of EGFP plasmid:shRNA (4 µg DNA total); for details of the EGFP nuclear expression plasmid and Fat1, Fat4 and control shRNAs (including validation in HEK293 cells), see the supplementary Methods. Five 50 ms pulses of 40-50 V with 950 ms intervals were delivered per embryo. Brains were dissected 3 days post-transfection and fixed in 4% paraformaldehyde at 4°C overnight, cryopreserved and sectioned coronally at 16 µm. The same anatomical level per embryo was analyzed using an Olympus IX81 inverted fluorescence microscope equipped with an Okogawa CSU X1 spinning disk confocal scan head. A total of three to four sections were analyzed per embryo, and at least three embryos per condition. Stitching of 20× objective images was performed using Volocity (PerkinElmer) software. VZ, SVZ and CP layers were delineated using Hoechst staining.

Co-immunoprecipitation analyses

Cell lines, the lysis protocol and western blot for Fat4 and Mupp1 and for Fat4 and Fat1 co-immunoprecipitation analyses are described in the supplementary Methods.

Determining the interactome of Fat1 and Fat4

Affinity purification and identification by mass spectrometry of Fat1 and Fat4 interaction partners were performed as detailed in the supplementary Methods.

Statistics

Data are expressed as mean±s.e.m. and were tested for statistical significance with Student's *t*-tests unless otherwise indicated, in which case they were analyzed by Student-Newman-Keuls post-hoc ANOVA. $P<0.05$ was considered significant. Tests were performed using Excel (Microsoft) or Prism5 (GraphPad).

Acknowledgements

We thank Dr Charles ffrench-Constant and Dr Phillipe Gros for *Fat1* and *Vangl2* mutant mice, respectively; Dr Gertler for providing Mena antibody; and Dr Gessler for the *Fat1 in situ* probe plasmid.

Competing interests

The authors declare no competing or financial interests.

Author contributions

Treatment and analyses of all mutant mouse embryos were performed by C.B. under the supervision of H.M. M.Z. performed all *in utero* experiments, procedures and analyses, under the supervision of F.M. R.S. first identified the Fat1 and Fat4 interaction. N.L. performed the Mupp1/Mena immunoprecipitation experiments. Analysis of Fat1 expression was performed by C.B. and M.B.-L. Mass spectrometry analysis was performed by E.C. and B.R. All authors wrote the paper.

Funding

This work was funded by Canadian Institutes of Health Research (CIHR) grants [MOP-38021 to F.M. and MOP-84468 to H.M.]. F.M. is an HHMI Senior International Research Scholar and holds a Canada Research Chairs (CRC) Chair. This work was funded by CIHR to H.M. Deposited in PMC for release after 6 months.

Supplementary material

Supplementary material available online at
http://dev.biologists.org/lookup/suppl/doi:10.1242/dev.123539/-/DC1

References

Barnabe-Heider, F., Wasylnka, J. A., Fernandes, K. J., Porsche, C., Sendtner, M., Kaplan, D. R. and Miller, F. D. (2005). Evidence that embryonic neurons regulate the onset of cortical gliogenesis via cardiotrophin-1. *Neuron* **48**, 253-265.

Bossuyt, W., Chen, C.-L., Chen, Q., Sudol, M., McNeill, H., Pan, D., Kopp, A. and Halder, G. (2014). An evolutionary shift in the regulation of the Hippo pathway between mice and flies. *Oncogene* **33**, 1218-1228.

Bultje, R. S., Castaneda-Castellanos, D. R., Jan, L. Y., Jan, Y.-N., Kriegstein, A. R. and Shi, S.-H. (2009). Mammalian Par3 regulates progenitor cell asymmetric division via notch signaling in the developing neocortex. *Neuron* **63**, 189-202.

Cappello, S., Gray, M. J., Badouel, C., Lange, S., Einsiedler, M., Srour, M., Chitayat, D., Hamdan, F. F., Jenkins, Z. A., Morgan, T. et al. (2013). Mutations in genes encoding the cadherin receptor-ligand pair DCHS1 and FAT4 disrupt cerebral cortical development. *Nat. Genet.* **45**, 1300-1308.

Caruso, N., Herberth, B., Bartoli, M., Puppo, F., Dumonceaux, J., Zimmermann, A., Denadai, S., Lebossé, M., Roche, S., Geng, L. et al. (2013). Deregulation of the protocadherin gene FAT1 alters muscle shapes: implications for the pathogenesis of facioscapulohumeral dystrophy. *PLoS Genet.* **9**, e1003550.

Chenn, A. and Walsh, C. A. (2002). Regulation of cerebral cortical size by control of cell cycle exit in neural precursors. *Science* **297**, 365-369.

Ciani, L., Patel, A., Allen, N. D. and ffrench-Constant, C. (2003). Mice lacking the giant protocadherin mFAT1 exhibit renal slit junction abnormalities and a partially penetrant cyclopia and anophthalmia phenotype. *Mol. Cell. Biol.* **23**, 3575-3582.

Clark, B. S., Cui, S., Miesfeld, J. B., Klezovitch, O., Vasioukhin, V. and Link, B. A. (2012). Loss of Llgl1 in retinal neuroepithelia reveals links between apical domain size, Notch activity and neurogenesis. *Development* **139**, 1599-1610.

Copp, A. J. (2005). Neurulation in the cranial region - normal and abnormal. *J. Anat.* **207**, 623-635.

Copp, A. J. and Greene, N. D. (2010). Genetics and development of neural tube defects. *J. Pathol.* **220**, 217-230.

Englund, C., Fink, A., Lau, C., Pham, D., Daza, R. A. M., Bulfone, A., Kowalczyk, T. and Hevner, R. F. (2005). Pax6, Tbr2, and Tbr1 are expressed sequentially by radial glia, intermediate progenitor cells, and postmitotic neurons in developing neocortex. *J. Neurosci.* **25**, 247-251.

Feng, Y. and Irvine, K. D. (2009). Processing and phosphorylation of the Fat receptor. *Proc. Natl. Acad. Sci. USA* **106**, 11989-11994.

Fietz, S. A. and Huttner, W. B. (2011). Cortical progenitor expansion, self-renewal and neurogenesis—a polarized perspective. *Curr. Opin. Neurobiol.* **21**, 23-35.

Gauthier, A. S., Furstoss, O., Araki, T., Chan, R., Neel, B. G., Kaplan, D. R. and Miller, F. D. (2007). Control of CNS cell-fate decisions by SHP-2 and its dysregulation in Noonan syndrome. *Neuron* **54**, 245-262.

Hildebrand, J. D. and Soriano, P. (1999). Shroom, a PDZ domain–containing actin-binding protein, is required for neural tube morphogenesis in mice. *Cell* **99**, 485-497.

Hou, R. and Sibinga, N. E. S. (2009). Atrophin proteins interact with the Fat1 cadherin and regulate migration and orientation in vascular smooth muscle cells. *J. Biol. Chem.* **284**, 6955-6965.

Ishiuchi, T., Misaki, K., Yonemura, S., Takeichi, M. and Tanoue, T. (2009). Mammalian Fat and Dachsous cadherins regulate apical membrane organization in the embryonic cerebral cortex. *J. Cell Biol.* **185**, 959-967.

Kibar, Z., Vogan, K. J., Groulx, N., Justice, M. J., Underhill, D. A. and Gros, P. (2001). Ltap, a mammalian homolog of Drosophila Strabismus/Van Gogh, is altered in the mouse neural tube mutant Loop-tail. *Nat. Genet.* **28**, 251-255.

Komatsu, Y., Kishigami, S. and Mishina, Y. (2014). In situ hybridization methods for mouse whole mounts and tissue sections with and without additional beta-galactosidase staining. *Methods Mol. Biol.* **1092**, 1-15.

Lake, B. B. and Sokol, S. Y. (2009). Strabismus regulates asymmetric cell divisions and cell fate determination in the mouse brain. *J. Cell Biol.* **185**, 59-66.

Mao, Y., Mulvaney, J., Zakaria, S., Yu, T., Morgan, K. M., Allen, S., Basson, M. A., Francis-West, P. and Irvine, K. D. (2011). Characterization of a Dchs1 mutant mouse reveals requirements for Dchs1-Fat4 signaling during mammalian development. *Development* **138**, 947-957.

Marthiens, V. and ffrench-Constant, C. (2009). Adherens junction domains are split by asymmetric division of embryonic neural stem cells. *EMBO Rep.* **10**, 515-520.

Matakatsu, H. and Blair, S. S. (2012). Separating planar cell polarity and Hippo pathway activities of the protocadherins Fat and Dachsous. *Development* **139**, 1498-1508.

Menzies, A. S., Aszodi, A., Williams, S. E., Pfeifer, A., Wehman, A. M., Goh, K. L., Mason, C. A., Fassler, R. and Gertler, F. B. (2004). Mena and vasodilator-stimulated phosphoprotein are required for multiple actin-dependent processes that shape the vertebrate nervous system. *J. Neurosci.* **24**, 8029-8038.

Mitchell, L. E. (2005). Epidemiology of neural tube defects. *Am. J. Med. Genet. C Semin. Med. Genet.* **135C**, 88-94.

Moeller, M. J., Soofi, A., Braun, G. S., Li, X., Watzl, C., Kriz, W. and Holzman, L. B. (2004). Protocadherin FAT1 binds Ena/VASP proteins and is necessary for actin dynamics and cell polarization. *EMBO J.* **23**, 3769-3779.

Nagy, A., Gertsenstein, M., Vintersten, K. and Behringer, R. (2007). Staining frozen mouse embryo sections for beta-galactosidase (lacZ) activity. *CSH Protoc.* **2007**, pdb.prot4726.

Pan, G., Feng, Y., Ambegaonkar, A. A., Sun, G., Huff, M., Rauskolb, C. and Irvine, K. D. (2013). Signal transduction by the Fat cytoplasmic domain. *Development* **140**, 831-842.

Rock, R., Schrauth, S. and Gessler, M. (2005). Expression of mouse dchs1, fjx1, and fat-j suggests conservation of the planar cell polarity pathway identified in Drosophila. *Dev. Dyn.* **234**, 747-755.

Saburi, S., Hester, I., Fischer, E., Pontoglio, M., Eremina, V., Gessler, M., Quaggin, S. E., Harrison, R., Mount, R. and McNeill, H. (2008). Loss of Fat4 disrupts PCP signaling and oriented cell division and leads to cystic kidney disease. *Nat. Genet.* **40**, 1010-1015.

Saburi, S., Hester, I., Goodrich, L. and McNeill, H. (2012). Functional interactions between Fat family cadherins in tissue morphogenesis and planar polarity. *Development* **139**, 1806-1820.

Shitamukai, A. and Matsuzaki, F. (2012). Control of asymmetric cell division of mammalian neural progenitors. *Dev. Growth Differ.* **54**, 277-286.

Sing, A., Tsatskis, Y., Fabian, L., Hester, I., Rosenfeld, R., Serricchio, M., Yau, N., Bietenhader, M., Shanbhag, R., Jurisicova, A. et al. (2014). The atypical cadherin fat directly regulates mitochondrial function and metabolic state. *Cell* **158**, 1293-1308.

Sopko, R. and McNeill, H. (2009). The skinny on Fat: an enormous cadherin that regulates cell adhesion, tissue growth, and planar cell polarity. *Curr. Opin. Cell Biol.* **21**, 717-723.

Sopko, R., Silva, E., Clayton, L., Gardano, L., Barrios-Rodiles, M., Wrana, J., Varelas, X., Arbouzova, N. I., Shaw, S., Saburi, S. et al. (2009). Phosphorylation of the tumor suppressor fat is regulated by its ligand Dachsous and the kinase discs overgrown. *Curr. Biol.* **19**, 1112-1117.

Staley, B. K. and Irvine, K. D. (2012). Hippo signaling in Drosophila: recent advances and insights. *Dev. Dyn.* **241**, 3-15.

Tanoue, T. and Takeichi, M. (2004). Mammalian Fat1 cadherin regulates actin dynamics and cell-cell contact. *J. Cell Biol.* **165**, 517-528.

Tissir, F. and Goffinet, A. M. (2013). Shaping the nervous system: role of the core planar cell polarity genes. *Nat. Rev. Neurosci.* **14**, 525-535.

Tsui, D., Vessey, J. P., Tomita, H., Kaplan, D. R. and Miller, F. D. (2013). FoxP2 regulates neurogenesis during embryonic cortical development. *J. Neurosci.* **33**, 244-258.

Van Hateren, N. J., Das, R. M., Hautbergue, G. M., Borycki, A.-G., Placzek, M. and Wilson, S. A. (2011). FatJ acts via the Hippo mediator Yap1 to restrict the size of neural progenitor cell pools. *Development* **138**, 1893-1902.

Viktorinova, I., Konig, T., Schlichting, K. and Dahmann, C. (2009). The cadherin Fat2 is required for planar cell polarity in the Drosophila ovary. *Development* **136**, 4123-4132.

Wang, X., Tsai, J.-W., LaMonica, B. and Kriegstein, A. R. (2011). A new subtype of progenitor cell in the mouse embryonic neocortex. *Nat. Neurosci.* **14**, 555-561.

Zhao, X., Yang, C.-h. and Simon, M. A. (2013). The Drosophila Cadherin Fat regulates tissue size and planar cell polarity through different domains. *PLoS ONE* **8**, e62998.

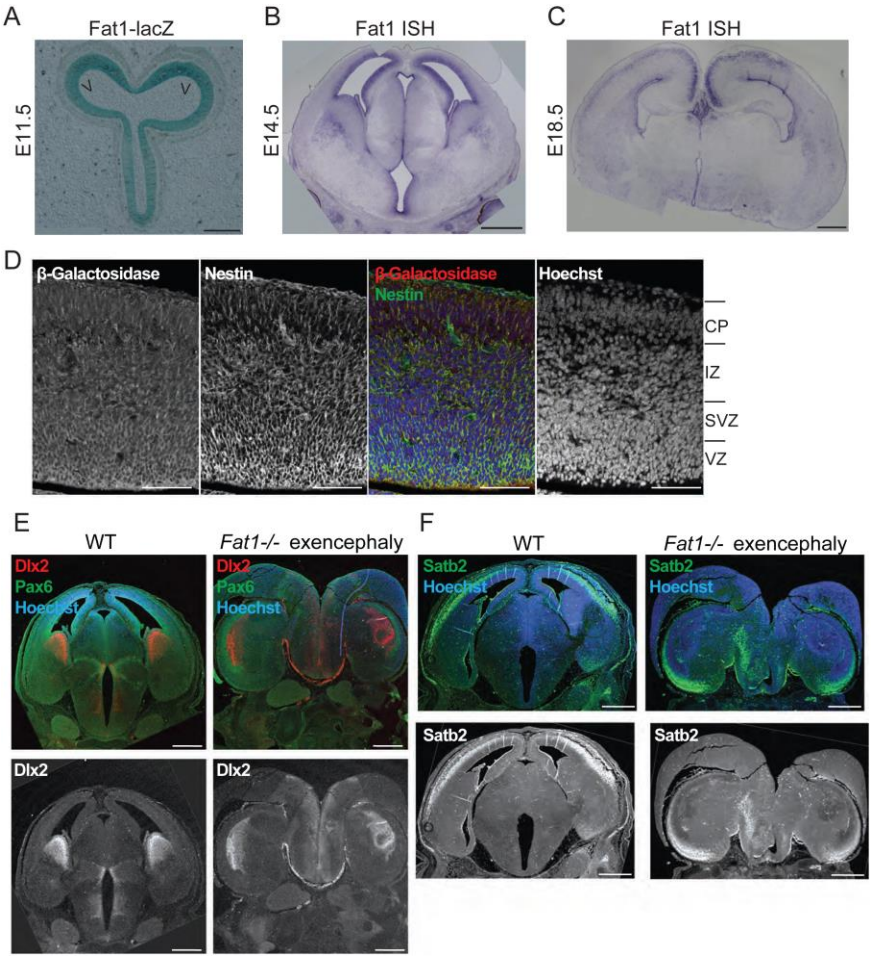

Figure S1. Fat1 is expressed in the developing brain

(A) Section through E11.5 *Fat1*$^{+/-}$ brain stained for β-Galactosidase to assess Fat1-lacZ expression. Scale bars, 100µm. (B,C) Fat1 expression in a coronal section from E14.5 (B) and E18.5 (C) brains revealed by in situ hybridization. Scale bar, 500µm. (D) Coronal section through E14.5 brain stained for β-Galactosidase (red) and the cortical precursor marker Nestin (green). Scale bars, 50µm. (E-F) Coronal section through E14.5 *Fat1*$^{-/-}$ exencephalic brain and control sibling stained for the ventral telencephalon marker Dlx2 (red) and the cortical precursor marker Pax6 (green) (E) and the neuronal marker Satb2 (green) (F) and Hoechst. Scale bars, 500µm. VZ, Ventricular Zone; SVZ, Sub-Ventricular Zone; IZ, Intermediate Zone; CP, Cortical plate.

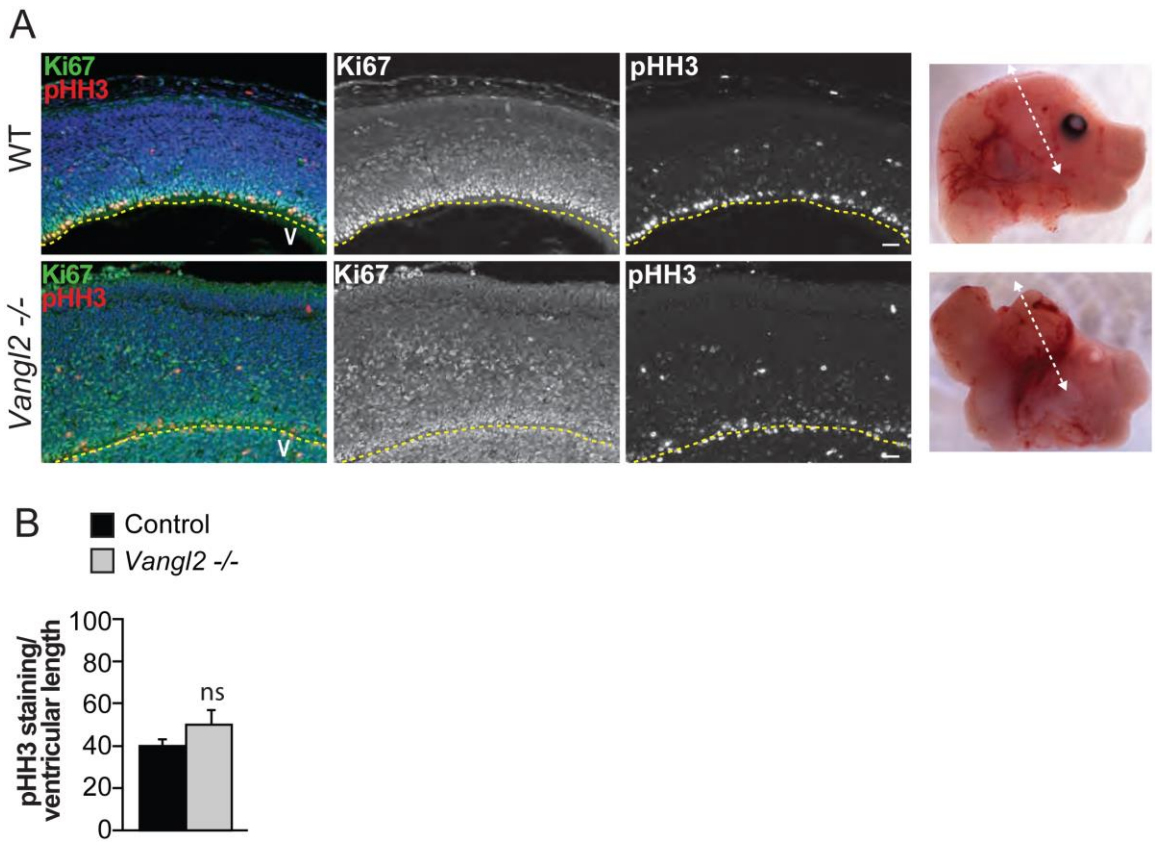

Figure S2. Proliferation of radial glial precursor is not increased in *Vangl2* mutants

(A) Confocal fluorescence micrographs from coronal sections of E14.5 *Vangl2*$^{-/-}$ embryos and a control sibling, stained for the proliferation marker Ki67 (green) and the mitotic marker pHH3 (red; left panel shows merge with hoechst). Corresponding embryos heads are on the right, with dashed arrows along the plane of sectioning. Capital V and yellow dashed line mark the ventricle. Scale bars, 20µm. (B) Quantification of the percentage of pHH3-positive cells calculated per ventricle length, in E14-15 *Vangl2*$^{-/-}$ embryonic cortices and control siblings. (n=5 controls and 4 *Vangl2* mutants, at least two different sections were measured for each).

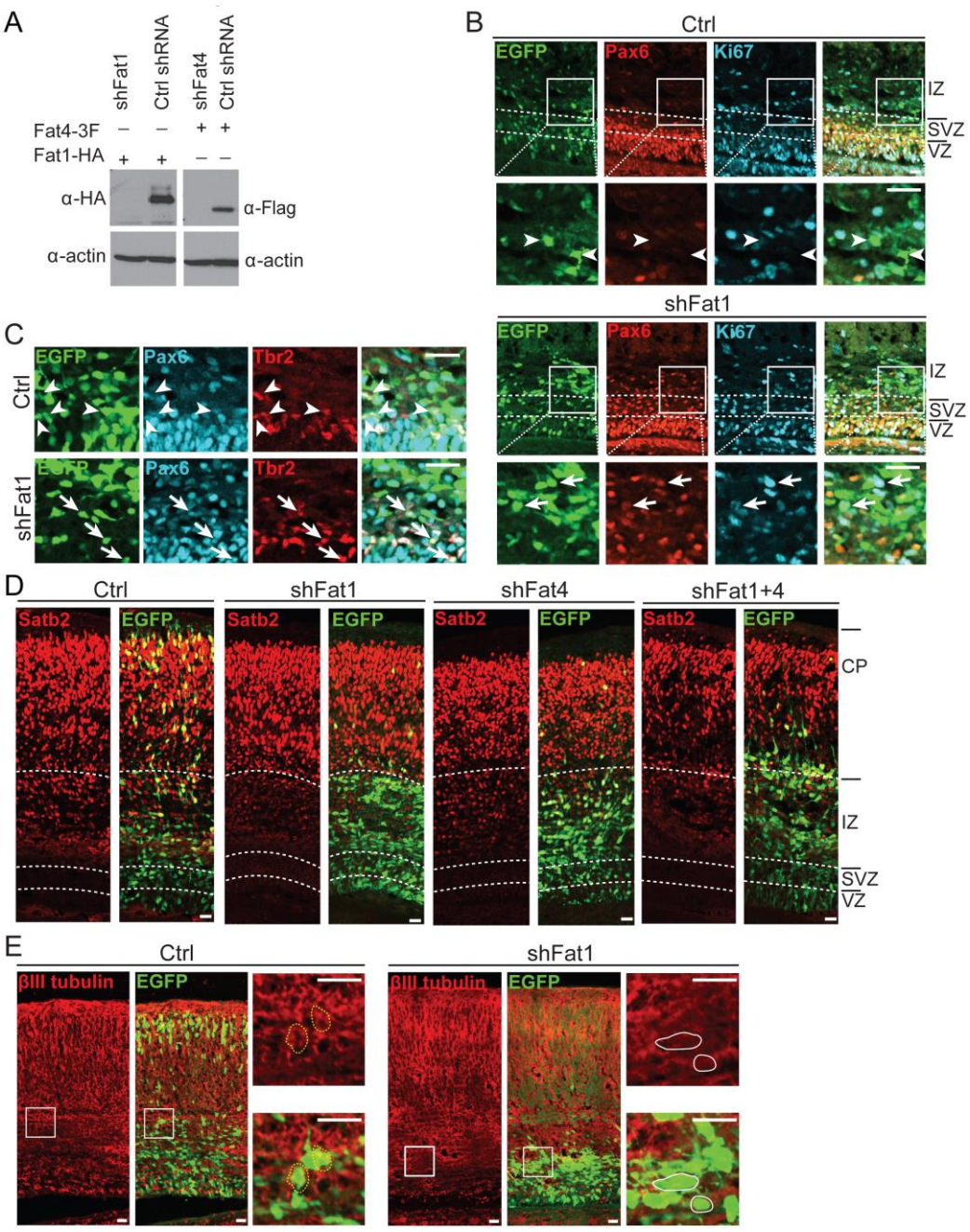

Figure S3.

(A) Western blot analysis of HEK 293 cell lysates after co-transfection with a Fat1-HA-tagged or a Fat4-Flag-tagged expression construct with Fat1 or Fat4 shRNAs. (B-E) E13/14 murine cortices electroporated with nuclear EGFP and a scrambled shRNA (Ctrl) or Fat1 shRNA (shFat1), and analyzed three days later at E16/17. (B) Confocal

fluorescence micrographs of coronal cortical sections immunostained for EGFP (green), Pax6 (red), and Ki67 (blue; right panel shows merge) . White lines demarcate different cortical regions, white boxes demarcate high magnification micrographs below. Arrows denote triple-labelled cells and arrowheads EGFP-positive cells negative for Pax6 and Ki67. Scale bar, 20μm. (C) Confocal micrographs of coronal sections immunostained for EGFP (green), Pax6 (blue), and Tbr2 (red; right panel shows merge). Arrows denote triple-labelled cells and arrowheads EGFP+, Pax6+ cells that are Ki67-negative. Scale bar, 20μm. (D) Low magnification fluorescence micrographs of coronal cortical sections immunostained for EGFP (green) and Satb2 (red). White lines demarcated different cortical regions. Scale bar, 20μm. (E) Fluorescence low maginification micrographs showing coronal cortical sections stained with βIII tubulin (red) and EGFP (green). White boxes demarcate high magnification micrographs below. White hatched line encircling EGFP+, βIII tubulin+ cells, white solid line encircling EGFP+, βIII tubulin-negative cells. Scale bar, 20μm.

A

129/B6

Genotype		Total Embryos	Exencephalic Embryos	% exencephalic
Fat1	*Fat4*			
Fat1 -/-	*Fat4 -/-*	0	0	**N/O**
Fat1 -/-	***Fat4 +/-***	**7**	**4**	**57%**
Fat1 -/-	***Fat4 +/+***	**5**	**1**	**20%**
Fat1 +/- or +/+	*Fat4 -/-*	8	0	**0%**
Fat1 +/- or +/+	*Fat4 +/- or +/+*	30	0	**0%**

CD-1

Fat1 -/-	*Fat4 -/-*	**15**	**4**	**27%**
Fat1 -/-	***Fat4 +/-***	**32**	**6**	**19%**
Fat1 +/-	***Fat4 -/-***	**44**	**1**	**2%**
Fat1 -/-	***Fat4 +/+***	**17**	**4**	**24%**
Fat1 +/+	*Fat4 -/-*	9	0	**0%**
Fat1 +/- or +/+	*Fat4 +/- or +/+*	159	0	**0%**

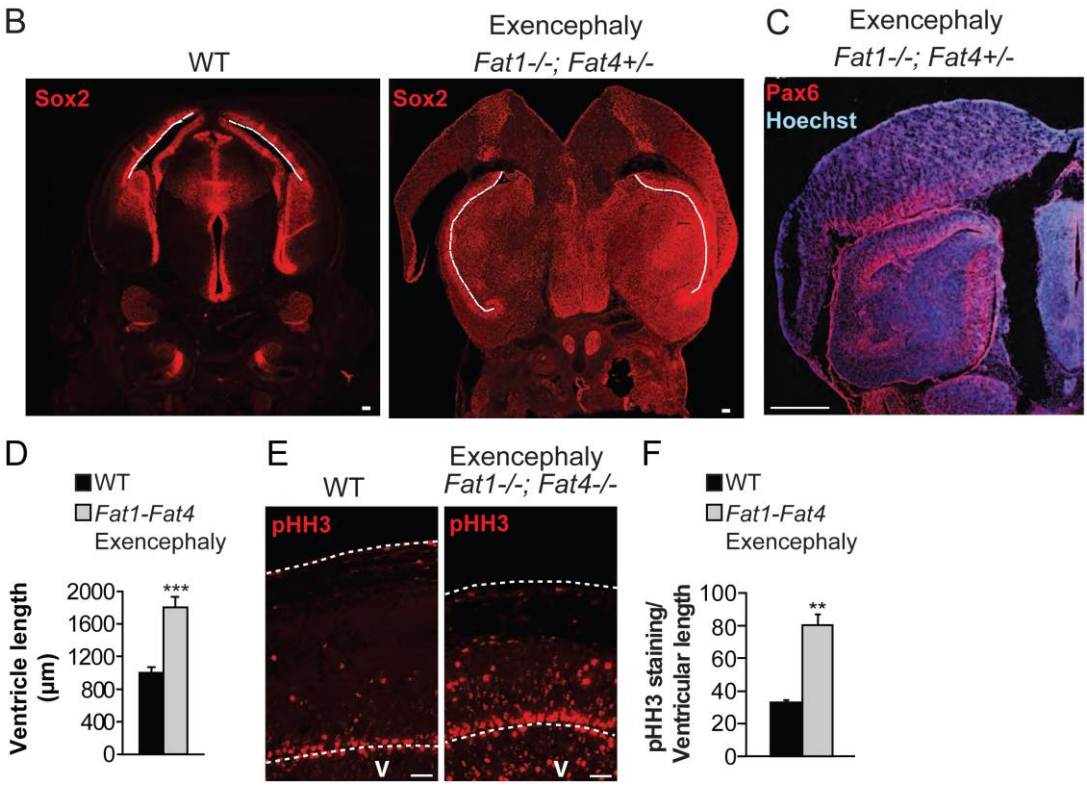

Figure S4. Loss of *Fat4* leads to an increase in the penetrance of *Fat1* exencephaly phenotype

(A) E13/15/16 embryos were obtained from *Fat1+/-; Fat4+/-* intercrosses in a mixed 129S6/SvEv - C57BL/6J (top) or in a CD-1 (bottom) genetic background. Numbers of progeny embryos with exencephaly are indicated for each genotype. N/O, non obtained

(B) Coronal sections from E15.5 *Fat1-/-; Fat4+/-* exencephalic brain and a control,

stained with Sox2. Dashed lines mark the lateral ventricles. (C) Coronal sections from E14.5 *Fat1-/-; Fat4+/-* exencephalic brain stained with Pax6. Sacle bar, 500µm (D) Quantification of posterior cortex length, from pictures similar to B and C (***p<0.001; n= 3 embryos each) (E) Coronal sections through E15.5 *Fat1-/-; Fat4+/-* exencephalic cortex and a control sibling stained for phospho-histone H3 (pHH3, red). Dashed lines indicate the apical (bottom) and basal (top) sides of the cortex. V, ventricle. (F) Quantification of the percentage of pHH3-positive cells calculated per ventricle length, from pictures as in E. Scale bars, 20µm (**p<0.01; n= 3 embryos each). Data are represented as mean ± SEM.

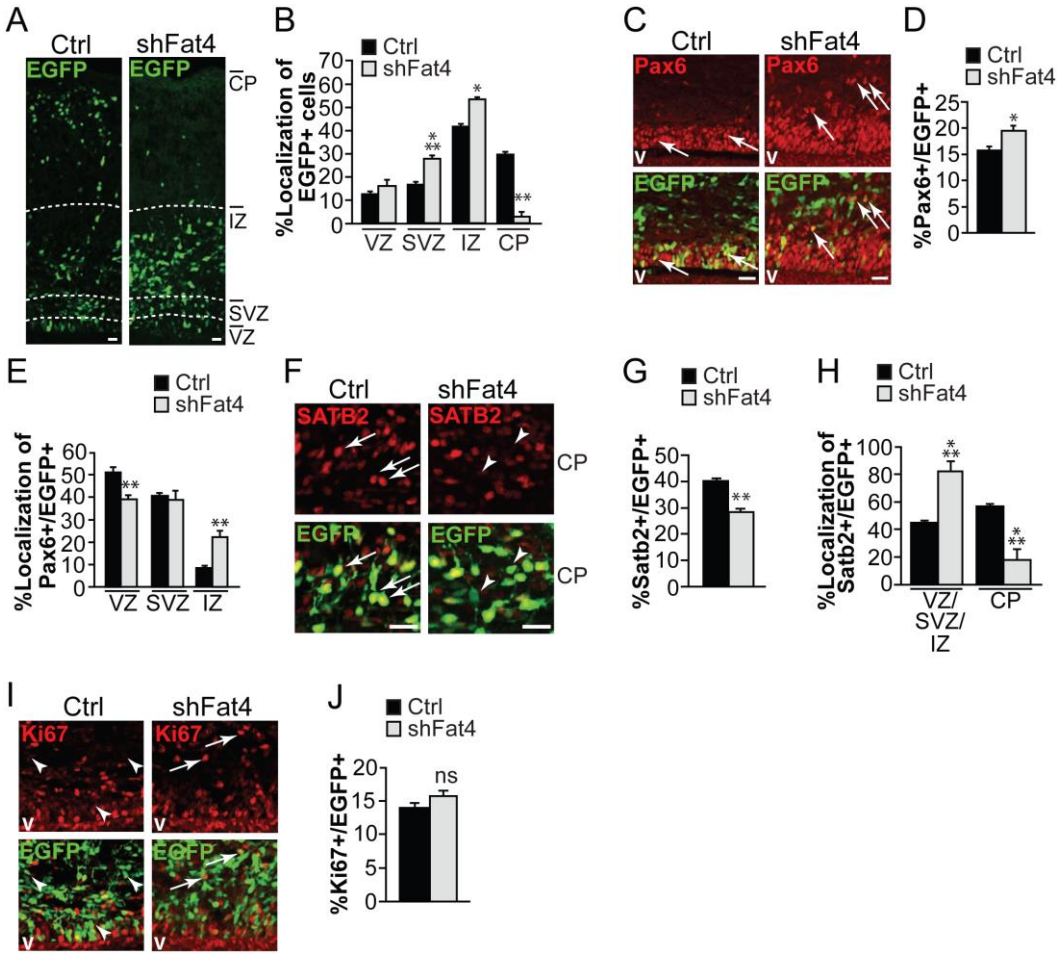

Figure S5. Fat4 knockdown promotes radial glial precursor proliferation

(A-J) Murine cortices were electroporated at E13.5 with a nuclear EGFP expression plasmid and Fat4 shRNA (shFat4) or a scrambled shRNA (Ctrl) plasmids, and analyzed three days later at E16/17. (A) Fluorescence confocal micrographs of E16.5 cortex stained for EGFP (green). Hatched white lines demarcate different cortical regions. (B) Quantification of sections as in A for the relative localization of EGFP positive cells. (*p<0.05; ***p<0.001; n=3 embryos each). (C) Confocal fluorescence micrographs from coronal sections through E16.5 cortex immunostained for Pax6 (red) and EGFP (green; lower panels show merge). (D,E) Quantification of sections as in (*C*) for the percentage

of Pax6+, EGFP+ cells per section (D) (*p<0.05), and relative localization in the VZ. SVZ, or IZ (E)(**p<0.01; n=3 embryos each). (F) Fluorescence confocal micrographs of the CP from coronal E16.5 cortical sections stained for Satb2 (red) and EGFP (green; right panel shows merge). (G,H) Quantification of sections as in (*F, S3D*) for the proportion of Satb2+, EGFP+ cells per section (G)(**p<0.01; n=3 embryos each), and relative localization in the VZ/SVZ/IZ versus the CP (H)(***p<0.001). (I) Fluorescence confocal micrographs of VZ/SVZ/IZ from coronal E16.5 cortical sections immunostained for Ki67 (red) and EGFP (green; lower panel shows merge). (J) Quantification of sections as in I for the proportion of Ki67+, EGFP+ cells per section. (n=3 embryos each). Arrowheads denote EGFP+ cells negative for respective marker and arrows denote double labelled cells. Scale bars, 20μm. ventricle; VZ, Ventricular Zone; SVZ, Sub-Ventricular Zone; IZ, Intermediate Zone; CP, Cortical plate. Error bars denote S.E.M.

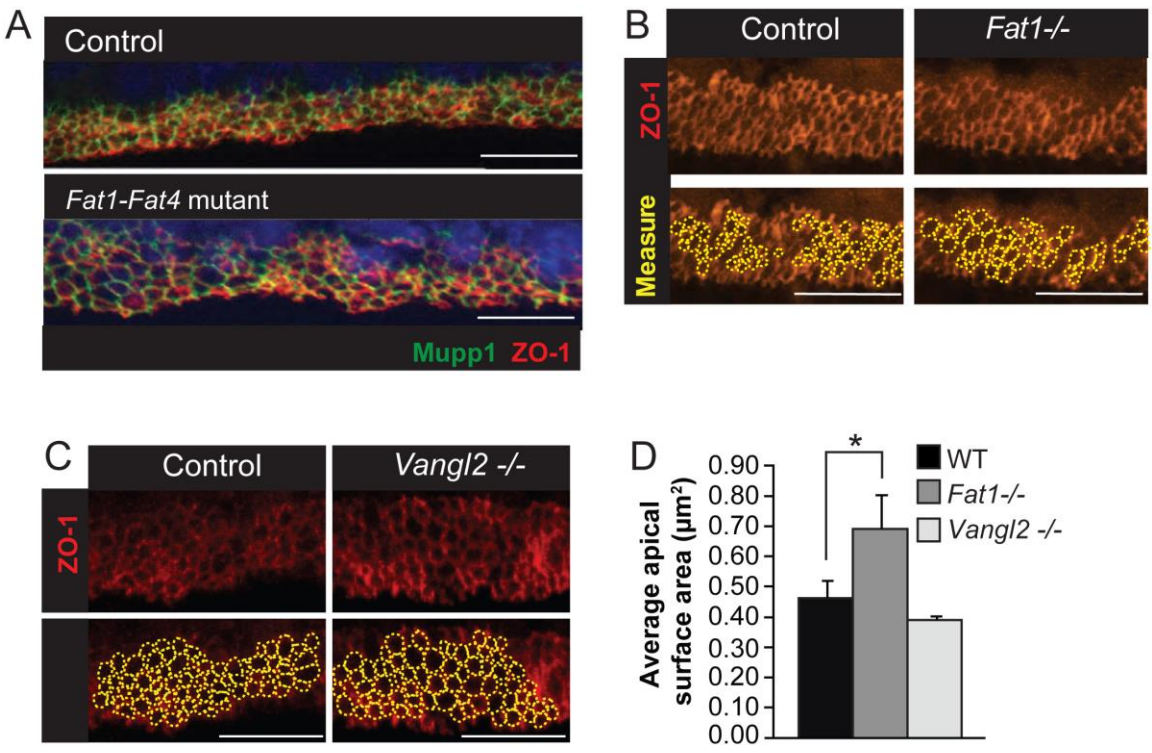

Figure S6. *Fat1* exencephalic mutants, but not *Vangl2*, have apical constriction defects

(A) Reconstruction of radial precursors apical surface in a *Fat1-/-; Fat4-/-* E14.5 cortex and a control sibling stained for ZO-1 (red) and Mupp1 (red). Scale bar, 5µm. (B,C) Radial glial progenitor apical domains 3D reconstructions from E14.5 *Fat1* exencephalic (B), *Vangl2* (C) mutants and controls, stained for ZO-1. Scale bar, 5µm. (C) Quantification of average apical surface area from images similar to those in B and C. (*$p<0.05$, n=10 control, n=4 *Fat1*$^{-/-}$ exencephalic embryos and n=4 *Vangl2*$^{-/-}$, at least 150 cells on 2 different sections were counted for each).

Protein	Top 4 control runs				FAT1-ICD run 1	FAT1-ICD run 2	FAT1-ICD SAINT	FAT4-ICD run 1	FAT4-ICD run 2	FAT4-ICD SAINT
KIF5B					920	875	**1.00**			
KLC2					695	667	**1.00**			
FAT1					**500**	**618**	**1.00**			
KIF5C					266	240	**1.00**			
KPNB1	26	20	5	2	205	180	**1.00**			
CSE1L					186	172	**1.00**			
PHB2					180	173	**1.00**			
PHB	4				113	108	**1.00**			
GCN1L1	5	4	2	2	73	44	**1.00**	14	4	
XPO1	1				69	61	**1.00**			
TNPO1					59	57	**1.00**			
ATAD3A	3				55	45	**1.00**	4		
RPN1	7				54	50	**1.00**		3	
PTPLAD1	13	4	4	2	51	46	**1.00**	12	13	
ATP5B	11	9	8	8	47	55	**1.00**	1		
C3orf39					47	37	**1.00**			
KLC1					44	46	**1.00**			
PEX19					31	23	**1.00**			
ATP5A1	9	8	6	5	29	28	**1.00**			
ATP2A2					27	31	**1.00**			
TNPO2					27	20	**1.00**			
ENAH					26	27	**1.00**			
IPO8					24	19	**1.00**			
KLC3					23	16	**1.00**			
HOMER1					21	19	**1.00**			
MTOR					20	9	**1.00**			
DCD	3	3	2	2	18	23	**1.00**			
SURF4					18	16	**1.00**			
VDAC2					17	13	**1.00**			
FIGF					17	12	**1.00**			
SEC61A1					14	13	**1.00**			
VDAC1					14	6	**1.00**			
XPOT					13	11	**1.00**			
STT3A					13	8	**1.00**	3		
FAT4								1176	1622	**1.00**
RPA1	10	3	2					165	154	**1.00**
LIX1L								107	97	**1.00**
DDX17	32	26	23	22	4	3		89	92	**1.00**
PARD3								85	81	**1.00**
RPS10-NUDT3	15	13	11	8	10	9		84	73	**1.00**
YBX1	31	19	18	17	21	23		82	90	**1.00**
C1QBP	10	9	6	6	9	7		82	84	**1.00**
TTC19								75	70	**1.00**
HSPD1	7	4	3	1	1			73	66	**1.00**
TIMM50	9	9	8	8	9	8		63	67	**1.00**
PMPCA								58	43	**1.00**
FRMPD1								57	42	**1.00**
USP9X								55	40	**1.00**
RPA3	7							45	35	**1.00**
PPP2R1A								45	34	**1.00**
SSBP1	6	4						43	45	**1.00**
BYSL	6	2						40	19	**1.00**
TRAF2								38	37	**1.00**
RPA2	2							34	24	**1.00**
FAM124A								34	21	**1.00**
PMPCB								31	34	**1.00**
PGAM5	3	3	1					31	31	**1.00**
MYL9								28	30	**1.00**
NOA1								23	46	**1.00**
PNMA2								23	19	**1.00**
CAD	3					2		23	13	**1.00**
CUL7								23	11	**1.00**
IGF2BP2								21	18	**1.00**
DNAJA3	4	2	2					18	18	**1.00**
MTDH	2							15	19	**1.00**
CDC20								15	16	**1.00**
C14orf169	1							14	12	**1.00**
AIM1								13	25	**1.00**
MOV10								13	7	**1.00**
MPP5								12	9	**1.00**
SND1								11	12	**1.00**
MPDZ								10	12	**1.00**
FBXW8								9	14	**1.00**
EMD	1							7	14	**1.00**
G3BP1	6	5	2					20	16	**0.99**
CALU	3					1		7	14	**0.98**
LARP1	5	3						12	14	**0.97**
EWSR1	7	7	6	5		1		27	18	**0.95**
IRS4	15	9	9	8				28	41	**0.94**
LUC7L3	7	7	3	3				18	14	**0.94**

Figure S7. Fat1 and Fat4 have different interactomes

MS data were analyzed as described in the text. Proteins identified with a SAINT score >0.9, and with >20 total peptides are shown. Known FAT1/4 binding partners are highlighted in blue. Proteins implicated in actin dynamics and junctions are highlighted in green. Bait proteins are highlighted in orange.

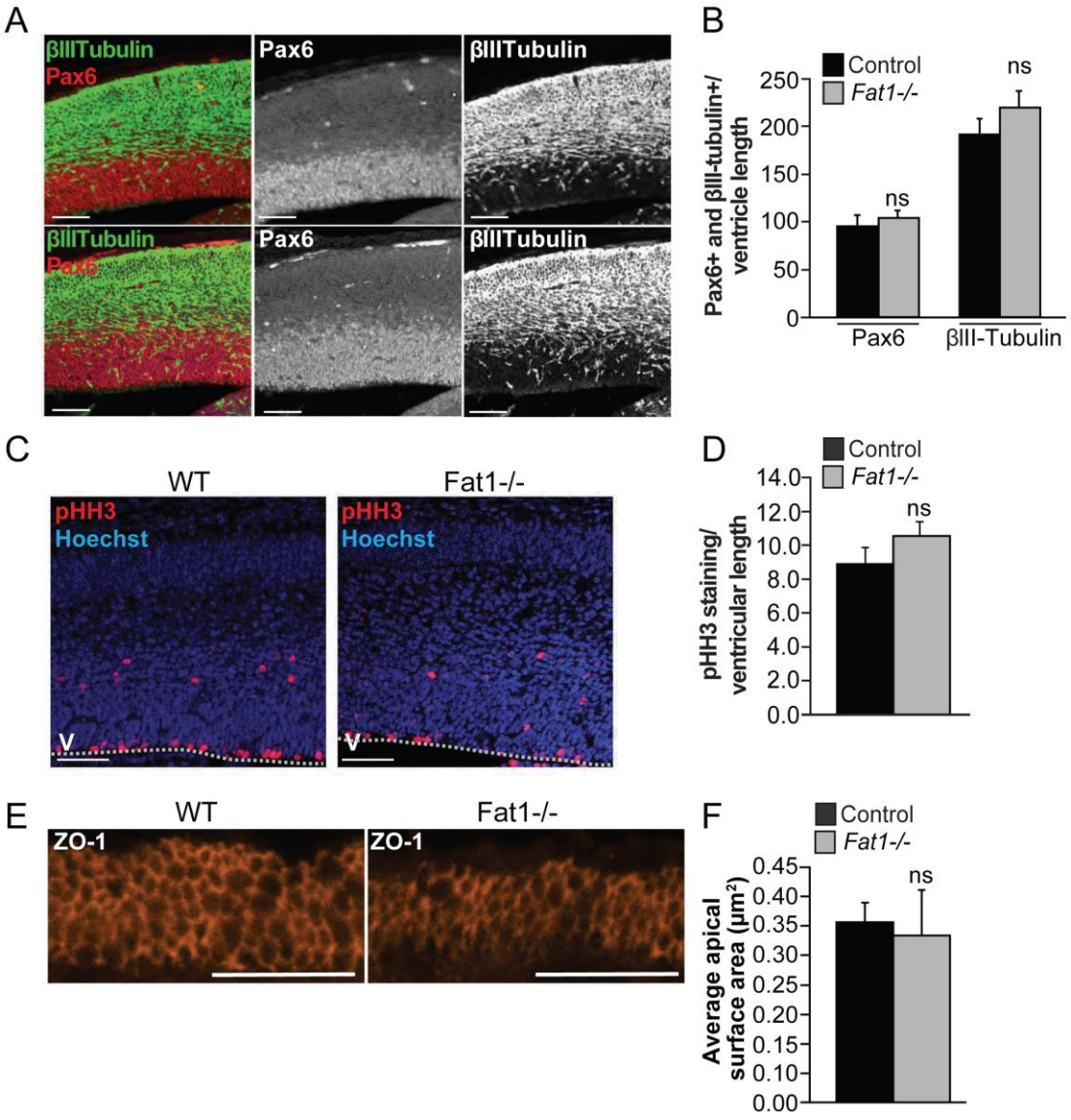

Figure S8. No increase in apical constriction or precursor proliferation in *Fat1* non exencephalic mutants

(A) Fluorescence confocal micrographs of *Fat1* non exencephalic mutant and control E14.5 cortex stained for Pax6 (red) and BIII-Tubulin (green). Scale bar, 100μm (B) Quantification of the percent Pax6+ and bIII-Tubulin+ areas in the dorsal cortex,

quantified from pictures as in A (n=3 embryos each). (C) Coronal sections through E14.5 *Fat1-/-* non exencephalic cortex and a control sibling stained for phospho-histone H3 (pHH3, red). Dashed lines indicate the basal side of the cortex. V, ventricle. Scale bar, 50µm (D) Quantification of the percentage of pHH3-positive cells per section calculated per ventricle length, from pictures as in C (n=3 embryos each). (E) Radial glial progenitor apical domains 3D reconstructions from E14.5 *Fat1* non exencephalic and control sibling, stained for ZO-1. Scale bar, 5µm. (F) Quantification of average apical surface area from images similar to those in C. (n=3 embryos each, at least 150 cells on 2 different sections were counted for each). Data are represented as mean ± SEM.

Supplementary Methods

Mouse lines

The *Fat4*$^{2E11\ \Delta flox}$ allele was described previously (Saburi et al., 2008). *Fat1lacZneo* mice were a gift from Dr. Charles ffrench-Constant (University of Edinburgh, UK). *Vangl2*^{Lp} (*Vangl2*^{S464N}) mice were generously provided by Dr Phillipe Gros (McGill University, Canada). Mice were maintained by backcrossing to 129S6/SvEv, CD-1 or C57BL/6J inbred mice (The Jackson Laboratory, USA).

Antibodies for immunostaining

The following primary antibodies were used in this study: rabbit anti-GFP (1:5000; Abcam #ab290), chicken anti-GFP (1:1000; Abcam #ab13970), rabbit anti-Pax6 (1:1000; Covance #PRB-278P), rabbit anti-Tbr2 (1:250; Abcam #ab23345), mouse anti-Satb2 (1:400; Abcam #ab51502), mouse anti-Ki67 (1:200; BD Biosciences #550609), rabbit anti-Sox2 (1:200, Cell Signaling #3728S), rabbit anti-pHH3 (1:500; Millipore #MABE13), mouse anti-Zo-1 (1:500; Invitrogen #339100), rabbit anti-βGalactosidase (1:200; Invitrogen #A11132), mouse anti-Nestin (1:400; BD Bioscience #554002) and rabbit anti-Par3 (1:200, Millipore #07-330). Relevant Cy3- or FITC-conjugated secondary antibodies (Jackson Laboratories) were used for primary antibody detection.

ß-galactosidase (lacZ) staining of embryonic brains and sectioning

A protocol similar to Nagy et al. 2007 was followed with minor modifications (Nagy et al., 2007). Briefly, E14.5 brains were dissected out of the developing skull in cold PBS.

Embryonic brains were then fixed with 0.2% glutaraldehyde for 30min at room temperature. Subsequently, tissues were washed and permeabilized using a wash solution containing sodium deoxycholate (0.01%) and NP-40 (0.02%) with a pH of 8.4. Embryos were stained with an X-gal solution overnight at 4°C followed by a final overnight fixation with 4% PFA. For tissue embedding, brains were serially dehydrated and incubated in liquid paraffin overnight. Coronal sections of 10uM were carried out on a Leica microtome. The paraffin was cleared with Histo-Clear, rehydrated and counterstained with Fast Red. Sections were mounted and visualized on a bright-field microscope.

Plasmids

The nuclear EGFP expression plasmid was driven from the *EF1 α* promoter (pEF-EGFP), while the cytoplasmic EGFP expression plasmid was driven from the CAG promoter (pCAGGS-EGFP) as has been previously described (Wang et al., 2012). Fat1, Fat4 and scrambled negative control shRNAs were purchased from EZBiolabs (Carmel, IN) and expression of the targeted sequences was driven from the H1 promoter. The targeted sequences are 5'-GCAGAGGTTCAACCTGAATCA-3' for shFat1 and 5'-GCACAGATCCCTCTAGAATCT-3' for shFat4. The shRNA negative control target sequence is 5'-GTTCTCCGAACGTGTCACGT-3'.

Validation of Fat1 and Fat4 shRNA in HEK293 cells

HEK293 cells were grown to confluency and cotransfected with mouse Fat1 or Fat4 constructs lacking most of their extra-cellular domains, Fat1ΔECD and Fat4ΔECD. Cells

were co-transfected with Fat1, Fat4 or control shRNAs using Lipofectamine 2000 (Invitrogen). shRNA targeting the C-terminal part of Fat1 and Fat4 cDNA were generated by EzBiolab.

Cell culture, co-immunoprecipitation and western blotting

For Fat4 and Mupp1 co-immunoprecipitation: Flp-In™ 293 T-Rex™ stable inducible cell lines expressing either FLAG-tagged Fat4 intracellular domain or GFP were cultured in DMEM mammalian media (Life Technologies) containing 10% fetal bovine serum (Sigma), 1% penicillin-streptomycin, 100ug/ml Hygromycin B (Bioshop) and 1% GlutaMAX media supplement (Life Technologies). Cells were induced with tetracycline (0.5 ug/ml for GFP, 1 ug/ml for Fat4) and harvested 48 hours after induction.

For Fat4 and Fat1 co-immunoprecipitation: HEK293T cells were transfected, using calcium phosphate transfection, with pCMV5 plasmids encoding Fat1ΔECD-HA, Fat4ΔECD-Flag, Fat4-ICD-Flag and BMPRII-Flag as indicated, 48 hours before lysis. Cells were lysed in buffer (50 mM HEPES [pH 8.0], 100 mM KCL, 2 mM EDTA, 0.1% NP40, 1.0 mM PMSF, 10% glycerol, and protease cocktail inhibitor [Roche]). FLAG-immunoprecipitation was performed by using α-FLAG M2 agarose beads (Sigma). SDS sample buffer was added after five washes of the beads with the lysis buffer. Western blots were performed according to standard protocols. Antibodies used were mouse α-FLAG (1:10000, Sigma #F1804), mouse α-MUPP1 (1:1000, BD Biosciences #611558), Rat α-HA (1:6000, Roche #11867431001) and mouse α-Mena (1:1000, gift from Gertler lab).

Affinity purification

For MS analysis of interacting proteins, 6 × 150 cm^2 dishes of sub-confluent (80%) HEK 293 cells expressing the protein of interest were scraped into PBS, pooled, washed twice in 25 ml PBS, and collected by centrifugation at 1000 × *g* for 5 min at 4°C. Cell pellets were stored at -80°C until lysis. The cell pellet was weighed, and 1:4 pellet weight:lysis buffer (by volume) was added. Lysis buffer consisted of 50 mM HEPES-NaOH (pH 8.0), 100 mM KCl, 2 mM EDTA, 0.1% NP40, 10% glycerol, 1 mM PMSF, 1 mM DTT and 1:500 protease inhibitor cocktail (Sigma-Aldrich, St. Louis, MO). On resuspension, cells were incubated on ice for 10 min, subjected to one additional freeze–thaw cycle, then centrifuged at 27000 × *g* for 20 min at 4°C. Supernatant was transferred to a fresh 15 ml conical tube, and 1:1000 benzonase nuclease (Novagen) plus 30 ul packed, pre-equilibrated Flag-M2 agarose beads (Sigma-Aldrich) were added. The mixture was incubated for 2 h at 4°C with end-over-end rotation. Beads were pelleted by centrifugation at 1000 × *g* for 1 min and transferred with 1 ml of lysis buffer to a fresh centrifuge tube. Beads were washed once with 1 ml lysis buffer and twice with 1 ml ammonium bicarbonate (ammbic) rinsing buffer (50 mM ammbic, pH 8.0, 75 mM KCl). Elution was performed by incubating the beads with 150 ul of 125 mM ammonium hydroxide (pH >11). The elution step was repeated twice, and the combined eluate centrifuged at 15000 × *g* for 1 min, transferred to a fresh centrifuge tube and lyophilized.

Mass spectrometry

One microgram of MS-grade TPCK trypsin (Promega, Madison, WI) dissolved in 70 ul of 50 mM ammbic (pH 8.3) was added to the Flag eluate and incubated at 37°C

overnight. The sample was lyophilized and brought up in 0.1% formic acid. LC analytical columns (75 um inner diameter) and pre-columns (100 um inner diameter) were made in-house from fused silica capillary tubing from InnovaQuartz (Phoenix, AZ) and packed with 100 Å C_{18}-coated silica particles (Magic, Michrom Bioresources, Auburn, CA). Peptides were subjected to nanoflow liquid chromatography - electrospray ionization - tandem mass spectrometry (nLC-ESI-MS/MS), using a 90 min reversed phase (10-40% acetonitrile, 0.1% formic acid) buffer gradient running at 250 nL/min on a Proxeon EASY-nLC pump in-line with a hybrid linear quadrupole ion trap (Velos LTQ) Orbitrap mass spectrometer (Thermo Fisher Scientific, Waltham, MA). A parent ion scan was performed in the Orbitrap, using a resolving power of 60,000. Simultaneously, up to the tweny most intense peaks were selected for MS/MS (minimum ion count of 1000 for activation) using standard CID fragmentation. Fragment ions were detected in the LTQ. Dynamic exclusion was activated such that MS/MS of the same *m*/*z* (within a 10 ppm window, exclusion list size 500) detected three times within 45 sec were excluded from analysis for 30 sec.

For protein identification, Thermo .RAW files were converted to the .mzXML format using Proteowizard (Kessner et al., 2008), then searched against Human RefSeq Version 45 (containing 36113 entries, appended with a reversed decoy database of equal size based on RefSeq v45) using the Comet (Eng et al., 2013) search engine. Search parameters specified a parent MS tolerance of 15 ppm and an MS/MS fragment ion tolerance of 0.4 Da, with up to two missed cleavages allowed for trypsin. Oxidation of methionine was allowed as a variable modification. Each AP was analyzed using at least two technical replicates. Statistical validation of peptide and protein identifications was

performed using the Trans-Proteomic Pipeline (Keller and Shteynberg, 2011). For each search, the Protein Prophet probability at 1% error rate was used as a cutoff value to generate a matrix input file to upload to the CRAPome (v1.1). 12 in-house control runs (consisting of Flag alone, Flag-GFP, and unrelated Flag-tagged proteins) and 30 additional control datasets were selected from within the CRAPome (all FLAG-AP/MS data in HEK 293 cells). SAINTexpress options were; LowMode = 0, MinFold = 0, Normalize = 1, Virtual controls = 4, Controls = All Controls.

BrdU incorporation

BrdU solution containing 5-Bromo-2′ -deoxyuridine (10 mg/ml) was injected intraperitoneally in pregnant mice (50 mg BrdU/kg of mice) 24 hours before embryonic dissection. The samples were prepared and sectioned as described above before being incubated overnight with anti-mouse BrdU antibody (Clone Bu20a, Dako).

Eng, J. K., Jahan, T. A. and Hoopmann, M. R. (2013) 'Comet: an open-source MS/MS sequence database search tool', *Proteomics* **13**(1): 22-4.
Keller, A. and Shteynberg, D. (2011) 'Software pipeline and data analysis for MS/MS proteomics: the trans-proteomic pipeline', *Methods Mol Biol* **694**: 169-89.
Kessner, D., Chambers, M., Burke, R., Agus, D. and Mallick, P. (2008) 'ProteoWizard: open source software for rapid proteomics tools development', *Bioinformatics* **24**(21): 2534-6.
Saburi, S., Hester, I., Fischer, E., Pontoglio, M., Eremina, V., Gessler, M., Quaggin, S. E., Harrison, R., Mount, R. and McNeill, H. (2008) 'Loss of Fat4 disrupts PCP signaling and oriented cell division and leads to cystic kidney disease', *Nature genetics* **40**(8): 1010-5.
Wang, J., Gallagher, D., DeVito, L. M., Cancino, G. I., Tsui, D., He, L., Keller, G. M., Frankland, P. W., Kaplan, D. R. and Miller, F. D. (2012) 'Metformin activates an atypical PKC-CBP pathway to promote neurogenesis and enhance spatial memory formation', *Cell stem cell* **11**(1): 23-35.